Hindawi
International Journal of Aerospace Engineering
Volume 2021, Article ID 8868797, 28 pages
https://doi.org/10.1155/2021/8868797

Research Article

Experimental Approach for the Evaluation of the Performance of a Satellite Module in the CanSat Form Factor for In Situ Monitoring and Remote Sensing Applications

Juan Sebastián Rodríguez,[1] **Andrés Yarce Botero**,[2] **Diego Valle**,[3] **Julián Gálvez- Serna**,[4] **and Francisco Botero**[1]

[1]*Applied Mechanics Research Group, Mechanical Engineering Department, Universidad EAFIT, Medellín 050022, Colombia*
[2]*Mathematical Modeling Research Group GRIMMAT, Mathematical Sciences Department, Universidad EAFIT, Medellín 050022, Colombia*
[3]*Group Bioinstrumentation and Clinical Engineering GIBIC, Bioengineering Department, Universidad de Antioquia, Medellín 050022, Colombia*
[4]*Faculty of Science and Engineering, Queensland University of Technology, Brisbane 4000, Australia*

Correspondence should be addressed to Juan Sebastián Rodríguez; jrodri36@eafit.edu.co

Received 6 August 2020; Revised 12 February 2021; Accepted 6 March 2021; Published 17 April 2021

Academic Editor: Seid H. Pourtakdoust

This article includes the phases of conceptualization and validation of a picosatellite prototype named Simple-2 for remote sensing activities using COTS (Commercial-Off-The-Shelf) components and the modular design methodology. To evaluate its performance and ensure the precision and accuracy of the measurements made by the satellite prototype, a methodology was designed and implemented for the characterization and qualification of CanSats (soda can satellites) through statistical tests and techniques of DoE (Design of Experiments) based on CubeSat aerospace standards and regulations, in the absence of official test procedures for these kinds of satellite form factor. For the above, two experimental units were used, and all the performance variables of the different satellite subsystems were discriminated. For the above, two experimental units were used, and all the performance variables of the different satellite subsystems were discriminated against. These were grouped according to the dependence of the treatments formulated in thermal and dynamic variables. For the tests of the first variables, a one-factor design was established using dependent samples on each of the treatments. Then, hypothesis tests were performed for equality of medians, using nonparametric analysis of the Kruskal-Wallis variance. Additionally, multivariate analysis of variance was carried out for nonparametric samples (nonparametric multivariate tests), and the application of *post hoc* multiple-range tests to identify the treatments that presented significant differences within a margin of acceptability. To know the dynamic response and ensure the structural integrity of the satellite module, shock, oscillation, and sinusoidal tests were applied through a shaker. Having applied the experimental methodology to the different units, the results of a real experiment are illustrated in which a high-altitude balloon was used through the application of nonparametric regression methods. This experiment's interest measured thermodynamic variables and the concentration of pollutants in the stratosphere to corroborate the operating ranges planned in the above experiments using on-flight conditions and estimate the TLR (technology readiness level) of future prototypes.

1. Introduction

CanSat is a picosatellite form factor (0.1-1 kg satellite classification by mass criterion). For almost 20 years, the CanSat concept has been used in the academic field for teaching space technology through hands-on activities and experiences, which can be enhanced and developed in more complex satellite missions for young students interested in

general science or engineering [1]. Thanks to work with CanSats, it is possible to transmit to students of diverse specialty basic concepts of design and construction of small artificial satellites as an educational strategy to generate interest among future generations of engineers and scientists in the space field [2]. The CanSat missions are interesting because they involve system integration, the definition of the protocols and the steps required for validating the integration of the mission subsystems, and the definitions of the integration tests required. For instance, the Education Office of ESA (European Space Agency) offers numerous research opportunities for universities and students from the member states, ranging from instruments and small platforms for satellites in terrestrial and lunar orbit, payloads in microgravity platforms, small satellite projects, and atmospheric balloons, which enables the validation of learning methods applied to engineering and knowledge/skill transfer models to students [3].

Although the CanSats have been known as "Sats," this term has been subject to discussion since there are no references to artifacts that, with this form factor, have managed to orbit the Earth or some other celestial body. However, in recent years, small satellites are being implemented a lot more in the space business [4]. One of the attributes of the nanosatellites and picosatellites is that they adopt a state-of-the-art commercial technology named COTS (Commercial-Off-The-Shelf), which allows new and less expensive ways of carrying out satellite missions with faster design and build [5]; this translates into a faster expansion of the technical and scientific knowledge and greater participation of the local industry [5]. The universities have been closely connected to these processes and have taken advantage of the technological advances in electronics, new materials, and more precise sensors to create smaller and technically simpler satellites with lower launch and operational costs. Equally, these resources enrich student training programs, stimulate their interest in a multidisciplinary technical environment for problem-solving, and have the necessary bases to face risks, with the extensive and necessary support from mentors, partners in industry, and institutions, among others [5].

Today, CanSats provide opportunities not only for training people in satellite issues but also for their low volume, their easy transportation, and installation which could be a suitable platform for the acquisition of information about a phenomenon and thus for carrying out geolocation activities and diverse *in situ* observations on multiple environments and scenarios. These prototypes consist of low-cost encapsulated systems that incorporate modular design methodology, which is not extensively used on the CanSat platform. This methodology pretends that the subsystems of the satellite are designed with the same communication bus and are not subject to the design of a single mission, for example, EPS (Electrical Power Supply), C&DH (Command and Data Handling), COMM (Communications), and ADCS (Attitude Determination and Control System). These subsystems are characterized by enabling the execution of functions for an experiment or a payload in particular and typically make up the architecture of any modern satellite system, such as CubeSats or satellites in a one-liter volume cube [6]. An exciting field for testing experimental payloads is the measurement of atmospheric variables through high-altitude balloons since they involve handling a large amount of data and maintaining a long-range telecommunication downlink. These types of activities constitute a relatively inexpensive way of applying what is known as hands-on space experiments while testing different components in environmental conditions similar to space, such as high radiation, high vacuum, and extreme temperatures. As an example of this, the LibreCube initiative seeks to develop CubeSat prototypes from OSS (Open-Source Software) and OSHW (Open-Source Hardware) [7]. However, they are mainly focused on space applications. In 2015, for instance, a demonstration experiment was carried out with a high-altitude balloon, reaching an altitude of over 30 kilometers and whose main payload was one of their prototypes. This experiment enabled the successful testing of the telemetry transmission received and postprocessed during the flight [8]. On the other hand, the upper atmosphere experimental data are useful for evaluating chemical transport models and are obtained through satellite data assimilation techniques, which improve the estimation of states and parameters provided by mathematical models [9].

The Simple-2 module (Figure 1) is a CanSat that emerged as an update of the Simple-1 module, developed by Semillero de Cohetería y Propulsion (Rocketry and Propulsion Study Research group) at Universidad EAFIT in 2016 and which was tested as a payload of a midpower rocket [10, 11]. The updates of the Simple-2 module involved the design of PCBs (Printed Circuit Boards) of multiple layers for the integration of SMD (surface mount device) components and the improvement of telecommunication integrating of a digital radio communication system for APRS (Automatic Packet Reporting System), which uses the AX.25 satellite communication protocol with the frequency modulation format AFSK (Audio Frequency-Shift Keying). The Simple-2 module is composed of four subsystems: *SimpleVital* as OB&DH; *SimplePollution* and *SimplePower* as EPS and payload subsystem on the same PCB, respectively; and the *SimpleRadio* as COMM.

Satellites with orbital capacity must comply with hard design constraints to withstand the space environment's severe conditions, given the impossibility of repairing the system in the event of failure. Therefore, the device's design and assembly must abide by strict safety criteria usually applied to electronic systems. This is particularly true when using COTS components and technology, which require the adoption of design techniques that guarantee system operation, even in the presence of device-level failures [2, 12, 13]. Currently, there are no clearly established standards for verifying the operability and performance of CanSats. However, the regulatory control of CubeSat design, qualification, and acceptance tests is generally applied from other specific standards of small satellites, except for the CubeSat/Deployer launch environment test according to ISO-17770:2017-space systems-cube satellites (CubeSats). Commonly, these tests seek to establish whether the main performance and functionality of all satellite subsystems comply with the design requirements in terms of testing in environment experiments. These include thermal-vacuum tests, useful for observing the state of thermal equilibrium and the performance of electronic components, examining

Figure 1: Prototype of CanSat Simple-2, which constitutes an experimental unit.

the thermal design and the surface material's properties to reveal design flaws in some of the subsystems and the vibration tests [14, 15]. Vibration tests are intended to check the mechanical strength of the satellite body and the safety of the same system in the event of losing parts or the malfunction of the deployment switches during the launch [16].

Although the regulations are clearly established for the CubeSat form factor, it was just possible to find a recent case study in which the tests described above were implemented in a CanSat prototype, demonstrating their effectiveness [2].

This study contributes to the development of a methodology (*how-know*) useful in future developments to test, to characterize, and to calibrate new CanSat platforms intended for obtaining *in situ* data and forecasting weather and environmental phenomena; it is also aimed at applying and/or adapting the current regulations for CubeSats, in line with experimental design techniques, and thus achieving statistical significance. The first part of the paper reviews the technical criteria of the Simple-2 module and each one of its specifications. In the second part, the experimental requirements, test environments, and theoretical framework are defined. The tests applied to two experimental units of CanSat Simple-2 are presented before analyzing the flight data obtained through a high-altitude balloon. Finally, the conclusions of this study and the recommendations for future work are presented.

2. CanSat Simple-2 Architecture

Surrey Satellite Technology Ltd. at the University of Surrey in the UK was a pioneer in the implementation of the modular design methodology, which enabled small satellites to gain enormous competitive advantages in the commercial arena [17]. Modular design methodology in satellites consists of integrating components with the same performance demands into a module where the structure must be adjusted to a standardized interface, which guarantees that the rest of the components coincide with mechanical and electrical terms [18]. The implementation of this approach also allows that a tested standard product supports a wide variety of missions.

Before defining the methodology to be implemented, it is essential to review each of the basic subsystems that make up a satellite prototype and define conceptually what will be a remote sensing system based on CanSats. Figure 2 describes each of the Simple-2 module subsystems, which are interconnected by a bus (SMD header) that used standard communication protocols to transmit data from the other subsystems to the *SimpleVital*. Inside the red boxes are the points on which the experimental strategy of the next section will focus.

The conceptualization of the CanSat Simple-2 design is a first approach to the use of modular design methodology whereby independent modules were conceived for the subsystems of OB&DH and COMM. It should be noted that to utilize the available volumes, the EPS and payload subsystems were designed in the same PCB, as mentioned above. In the next subsections, it will describe the characteristics of each subsystem.

2.1. SimpleVital: On-Board Data Handling (OB&DH). The OB&DH was responsible for managing, storing, and sending information that comes from the other electronic subsystems to the ground segment through the communication subsystem. This board (Figure 3) consists of an 8-bit microcontroller, communicated employing standard protocols such as Serial, I^2C (Interintegrated Circuit), and SPI (Serial Peripheral Interface) to peripheral units such as GPS (Global Positioning System), IMU (Inertial Measurement Unit), barometer, and temperature and communicates with external units such as the subsystems of EPS, payload, and COMM. This subsystem is also responsible for providing a format to the data for storage in an SD memory.

2.2. SimplePower: Electrical Power Supply (EPS). EPS regulates the power for satellite subsystems. In this module (Figure 4), the charge is stored in a one-cell LiPo (Lithium Polymer) battery with 1500 mAh. This battery supplies between 3 and 4.2 volts, which is regulated to 5 volts using a DC-DC upconverter and subsequently distributed to other subsystems. Depending on the radio transmitter used (UHF or VHF), the sensor configurations, and sample rate, the consumption managed by this subsystem was about 3 (Wh). Additionally, this subsystem controls the power supplied by the solar cells (solar array interfaces) through a direct energy transfer architecture [19]; this enables the extension of the operation time of the module thanks to the additional power already available in the batteries.

2.3. SimplePollution: Payload Subsystem. This subsystem was located on the same PCB of the EPS subsystem and is composed of a sensor that measures the concentration of gases (Figure 4(b)) such as CO (carbon monoxide), NO_2 (nitrogen

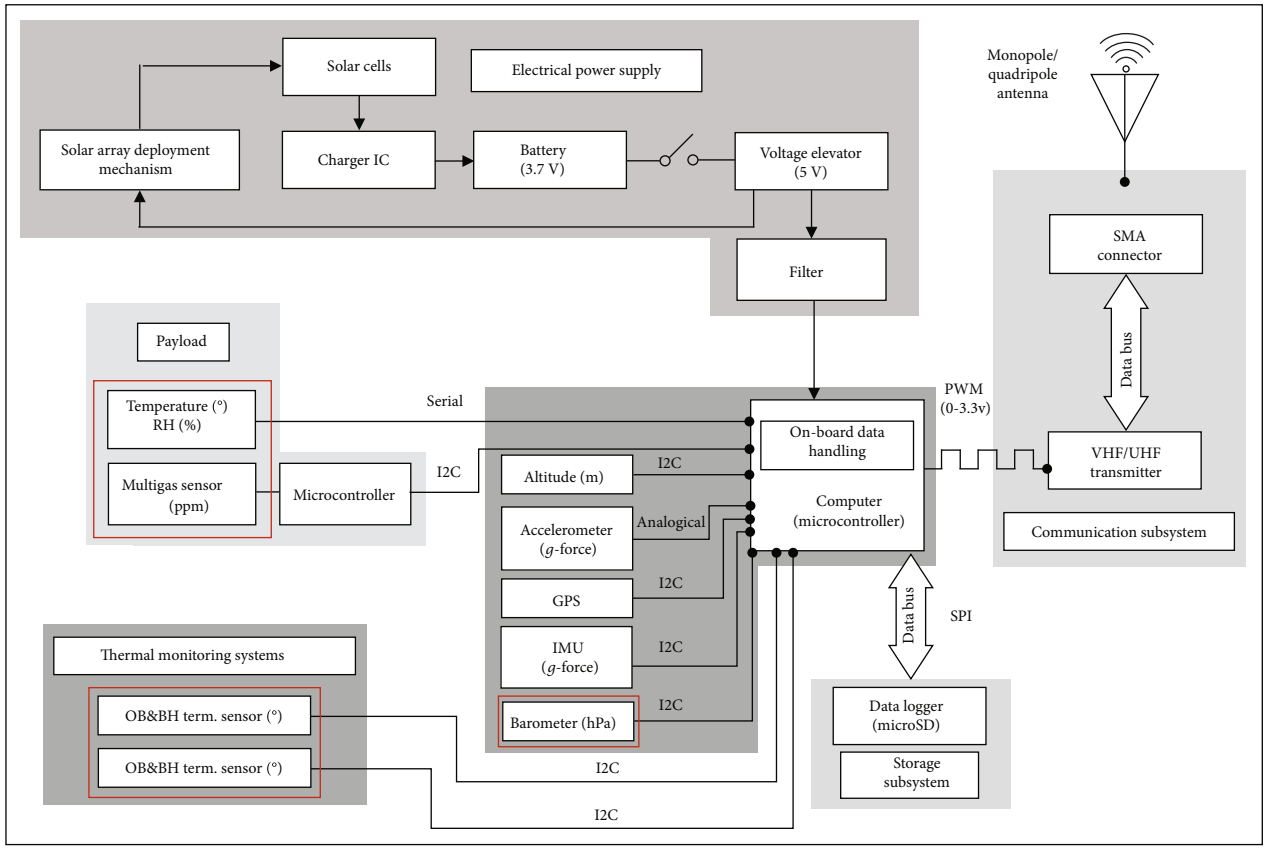

Figure 2: Block diagram of the subsystems of the Simple-2 module.

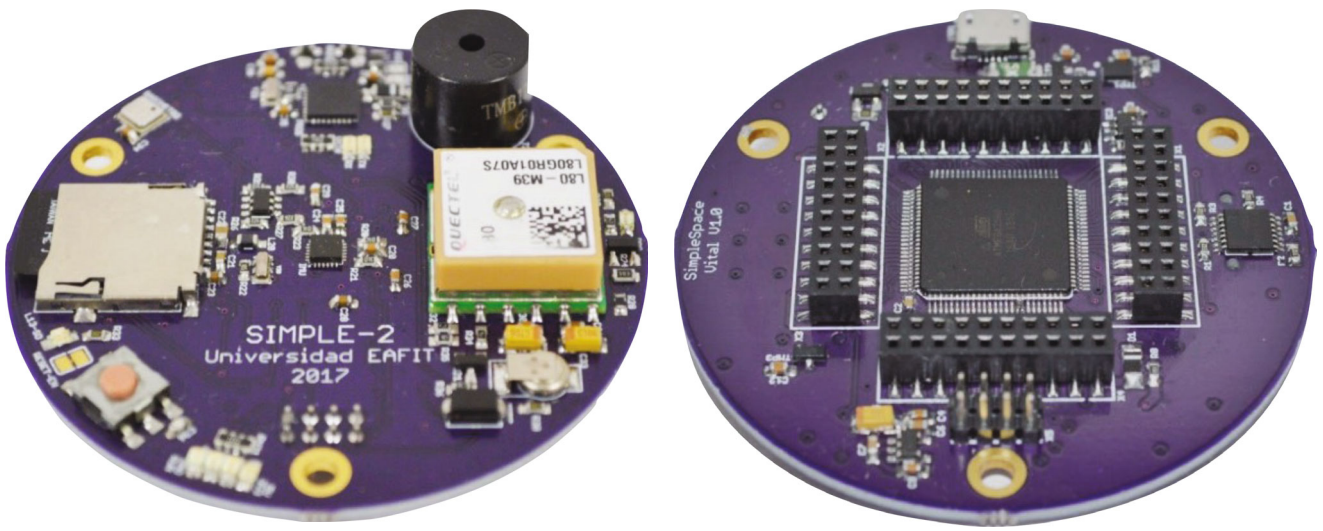

(a) (b)

Figure 3: *SimpleVital* board interface top (a) and bottom (b).

dioxide), C_2H_6OH (ethanol), H_2 (hydrogen), N_3 (ammonia), CH_4 (methane), C_3H_8 (propane), and C_4H_{10} (isobutane), in addition to physical quantities such as relative humidity and temperature.

2.4. SimpleRadio: Communication Subsystem. This subsystem is responsible for transmitting to the ground segment the information sent by the OB&DH via APRS protocol data frames in the UHF/VHF bands, using NB (narrow band) radio transmitters of 433.650 MHz @ 10 mW and 144.390 MHz @ 300 mW, respectively (Figure 5(a)).

2.5. Thermal Monitoring Systems. The thermal monitoring subsystem consists of three surface sensors distributed over

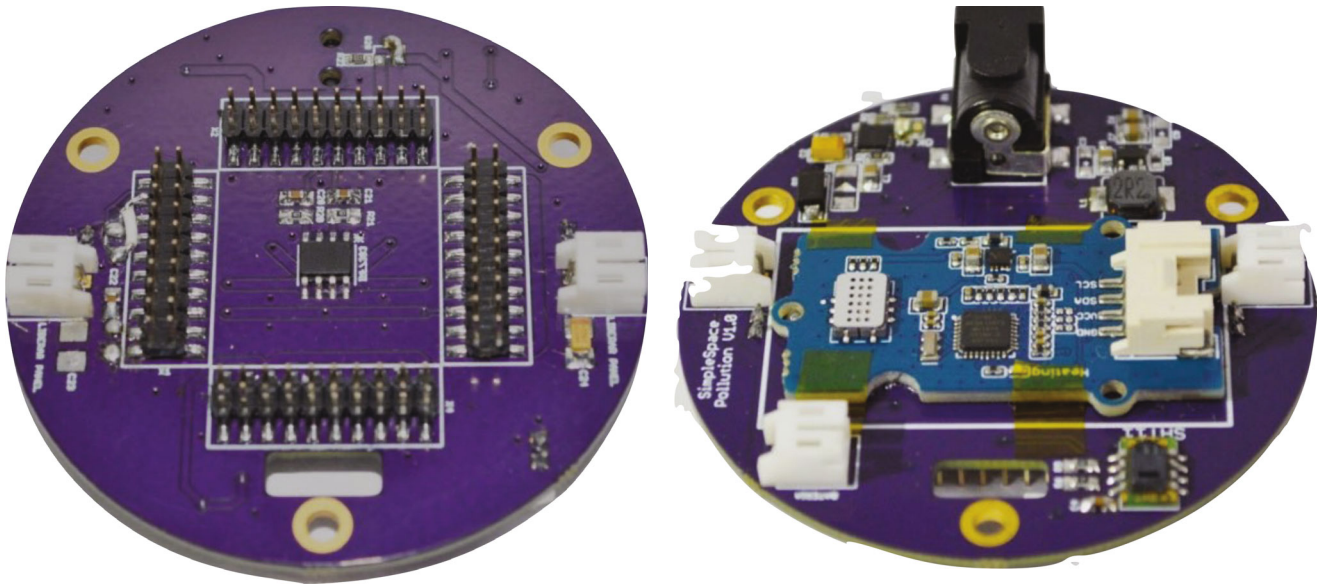

(a) (b)

Figure 4: *SimplePower* and *SimplePollution* both in the same board interface, top (a) and bottom (b).

the PCBs to measure the temperature corresponding to different points of interest in the other subsystems like EPS and OB&DH, as well as the environment temperatures.

3. Design of Experiments: Description and Theoretical Framework for Thermal-Vacuum and Flight Analysis

A one-factor design (single-factor design) uses a qualitative explanatory variable named factor. The values assumed by this factor are named levels. In the statistical model proposed, the levels are the different treatments applied to the experimental units [20]. The present experimental exploration is a one-factor design, given that there are limitations in the equipment for establishing the treatments, which in turn make it impossible to represent the main and interaction effects typical of factorial designs. In the case of linear models, the technique one-way ANOVA (analysis of variance) for a single-factor or one-factor design is widely used to know the variability observed in each of these treatments.

In cases where the data do not present normality and homoscedasticity conditions, the Kruskal-Wallis test, which is considered a homologous test to the one-way ANOVA, contrasts the hypothesis that given k quantitative samples come from or have been obtained from the same population. In this way, the hypotheses of the Kruskal-Wallis test are H_o, where the$k$medians are all equal and come from the same population, andH_a, where at least one of the$k$medians is different and does not come from the same population.

Additionally, this exploration contemplates the use of the NPMV (nonparametric multivariate) inference analysis technique since it supports cases in which there is more than one dependent variable that cannot be combined in a simple manner. The NPMV technique has the advantage of not taking on parametric assumptions like multivariable normality. These assumptions are required for the classical parametric MANOVA (multivariate analysis of variance), which are quite restrictive and challenging to verify [21]. In this case, the P values (probability values) are calculated for approximations of F (Fisher distributions), even for general and permutation tests, where the significant subsets of response variables and the factor levels are identified. Multivariate analysis techniques are used to determine if the independent variables' changes have significant effects on the dependent variables.

Additionally, these techniques also identify potential relationships between the independent variables and their association with the dependent variables [22]. In summary, Kruskal-Wallis tests the differences between two or more median groups, while the NPMV tests the difference of two or more vectors of means. Once the null hypothesis is rejected in the univariate and multivariate analyses, one-factor experiments involve multiple-range tests and sample comparison tests to identify which treatments and which dependent variables differ from each other.

The previous set of statistical inference tests enables collecting information on the experimental module's performance at the laboratory level and under controlled conditions. However, this module's real flight test will reveal that the nature of the variables of interest (thermodynamic and atmospheric variables) requires the nonlinear regression methods to predict their behavior and variability in relation to altitude changes.

It was decided to apply different nonparametric regression methods with a single predictor on the flight data set. Such methods substitute the linearity assumption by smoothness for the regression function [23].

It should be noted that, in most cases, the relationship between variables and atmospheric pollutants does not

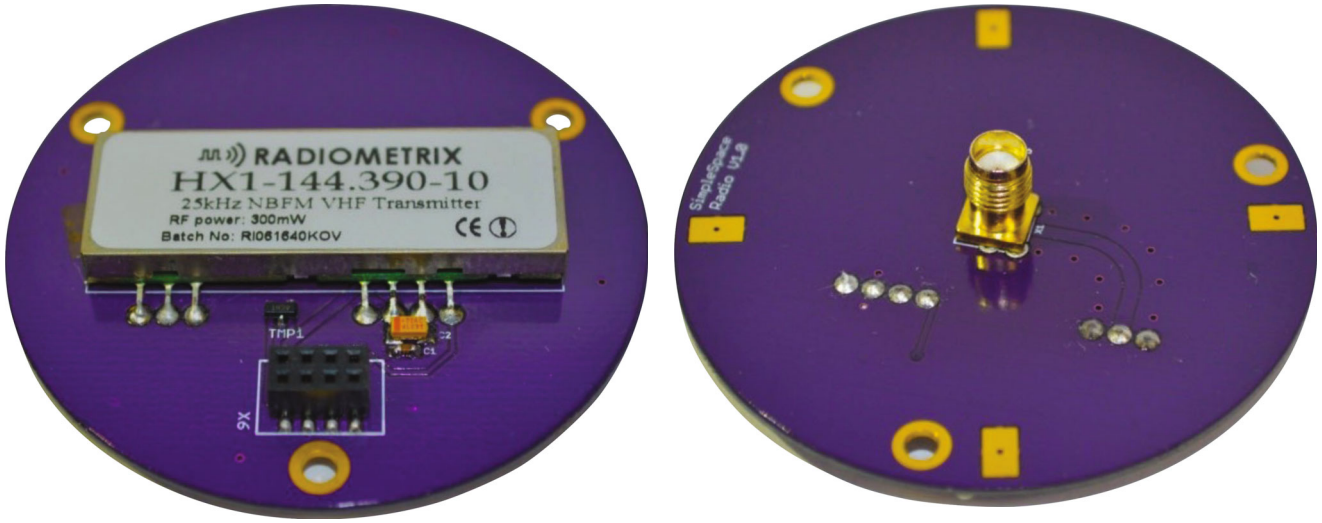

(a) (b)

Figure 5: *SimpleRadio* board interface top (a) and bottom (b).

always behave linearly. Its behavior is complex and is influenced by meteorological factors, by the characteristics of the emission sources, and by topographic aspects [24]. Therefore, parametric regression methods lose their validity compared with nonparametric methods since these model the behavior of a data set without assuming a known functional form *a priori* [25].

4. Methodology

The variables of interest for the experimental analysis are part of the subsystem of sensors (payload) and the subsystem of thermal monitoring, given that it constitutes the basic variables to understand aspects of meteorological phenomena close to the RS (Radiosonde Station) type [26]. In the experimental design, these variables are conceptualized as dependent on the treatments to be implemented, which are standard deviations of these variables, namely, $S_{T_1} = T_1$, $S_{T_2} = T_2$, $S_{T_3} = T_3$, $S_{T_4} = T_4$, $S_{\mathrm{RH}} = \mathrm{RH}$, and $S_P = P$. Such DV (dependent variables) will be defined in detail in Table 1.

As mentioned above, there are two main test environments: thermal-vacuum tests and vibration tests. In satellite prototypes, it is necessary to perform the first to control the outgassing of components and the nonvolatile residue limit of the payload, which allows confirming or not the functional and operational requirements in an appropriate environment (high- and low-temperature worst cases). The vibration tests seek to ensure the satellite's structural strength (dynamic loads), the determination of resonant frequencies and the resistance of the integrated circuits, their connections, and the materials' resistance to being subjected to mechanical stress during the launch.

These test environments consist of the set of external conditions that arise during the flight of aerospace vehicles. Each environment can be based on real flight data, analytical predictions, or a combination of both. The level of the expected extreme environment, used for the qualification tests, is P99/90, that is, one that does not exceed at least 99% of flights and is at least estimated with at least 90% of confidence. The maximum expected environment level used in acceptance tests is P95/50 [27]. In methodological terms, the dashed line boxes in Figure 6 represent each of the test environments on which an experimental strategy and/or qualification tests were applied.

It should be noted that the environment (1) corresponded to vacuum-thermal tests when the temperature is positive (temperature values over zero) because low-temperatures were not considered, while the test environment (2) consisted of vibration tests. It is important to mention that each of these tests was always accompanied by reference sensors to guarantee a calibration and traceability process. Section 7 will show the results of a real test environment that will be denoted by the number (3). The test environments (1) and (3) correspond to the scenarios where the statistical tests described in the previous section's theoretical framework were applied.

The DVs constitute a specific type of sensor selected not only for its commercial availability but also for its low-volume, low-mass, and low-power stored chemical energy consumption that will not exceed 100 watt-hours, just as indicated by the satellite standards for CubeSats [28]. The characteristics of these sensors have been listed in Table 1.

Once the sensors were identified for the variables to be analyzed, their readings were verified through the microcontroller of the board data handling subsystem. Then, these variables were graphed in real time. Once the signals stabilized by the reference temperature and pressure values, the preestablished treatments were applied in a thermal-vacuum chamber (see Figure 7). It should be noted that before these procedures, a sample size n was calculated according to the maximum error estimated for the mean population and according to the variance estimation. In the end, once all the samples dependent on each of the treatments were collected, hypothesis tests were carried out for the equality of means and medians, through univariate and multivariate analysis,

Table 1: Sensor datasheet corresponding to some dependent variables or response variables.

Nomenclature	Sensor	Reference	Protocol	Units/accuracy	Minimum range	Maximum range
T_1	Temperature	BMP180	I^2C	˚C, ±2.0	-40	+85
T_2	Temperature	AT30TSE004A	I^2C	˚C, ±3.0	-20	+125
T_3	Temperature	SHT11	Serial	˚C, ±0.4	-40	+123.8
RH%	Relative humidity	SHT11	Serial	%, ±0.1	0	100
P	Barometric pressure	BMP180	I^2C	hPa, ±0.02	300	1100

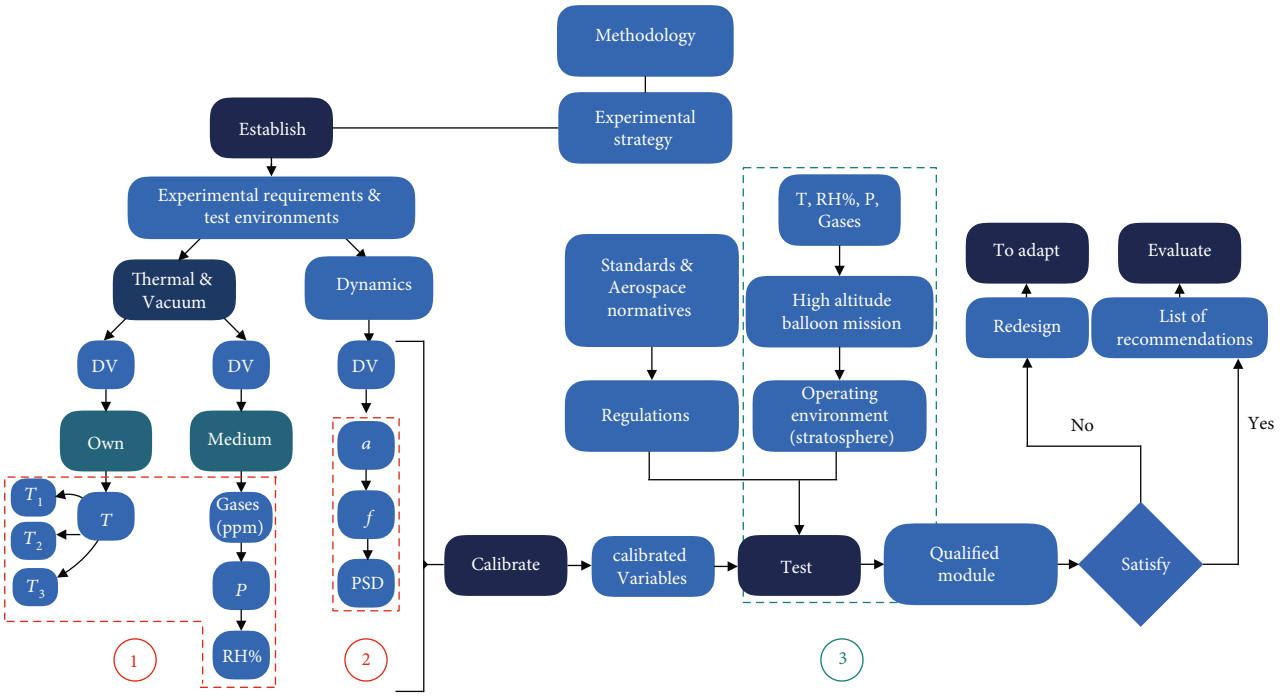

Figure 6: Methodology of blocks and experimental strategies. Dark blue boxes correspond to the goals to meet with the methodology. Blue boxes correspond to the different steps to meet the goals, and dashed line boxes frame the three test environments.

on which the individual verifications of assumptions and multiple-range tests were made to identify which treatments presented significant differences.

The confidence interval of the variance for each of the dependent variables was calculated to gather information about the measurements' variability to compare them with the equivalent calculations on the reference sensors. Finally and given the nature of the data obtained from the module ascent test employing a high-altitude balloon, the nonparametric regression methods described in Section 3 were used to determine the association between environmental variables and altitude changes.

5. Considerations for Thermal Drift Test

During the orbital cycle of a satellite, the temperature varies due to daylight alternation and Earth's shadow. However, the orbital period is short enough not to allow too much heat to accumulate or be released into space, preventing the satellite's burning or freezing. Some predicted external temperature ranges with active electronics are between -5 and +50 ˚C. It is necessary to specify that the parts subject to this range are peripheral, such as solar panels and antennas. The temperature range within the satellite is between +20 and +70 ˚C; hence, electronic circuits must comply with the characteristic of being compatible with standard commercial devices [12]. Some common thermal cycles may vary (Table 2), for instance, if it is for qualification model from -15 ˚C to +45 ˚C and for flight model (FM) from -10 ˚C to +35 ˚C [29].

To simulate conditions for complete cycles of operation, in terms of the temperature changes that a nanosatellite faces during the orbital period, positive thermal drift test stands are commonly used in conjunction with vacuum test stands [30]. Previous experiments revealed that it is not a problem when the electronic components are sealed about the vacuum test. However, the thermal power transmission capacity is reduced due to missing convection, leaving only conduction and radiation as heat transfer mechanisms to the outside [12]. In relation to this, thermal-vacuum tests were performed with a temperature range from +20 to +50˚C and a

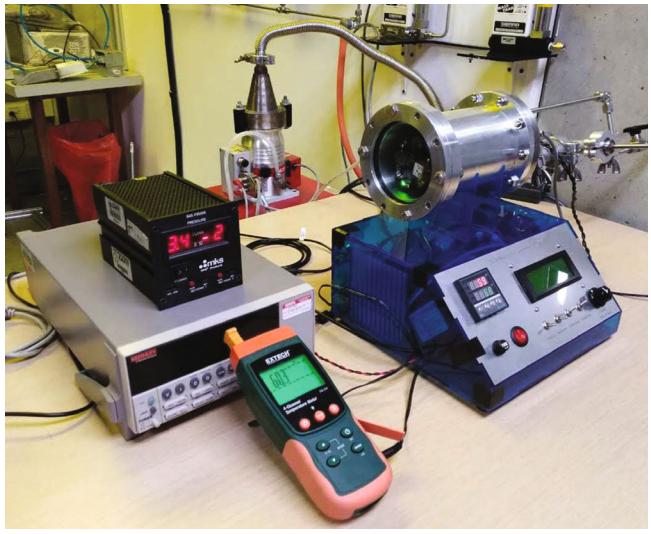

Figure 7: Thermal-vacuum chamber. Laboratory of Microengineering, Department of Physical Sciences at Universidad EAFIT.

Table 2: Some CubeSat projects and their respective common temperature ranges (maximum and minimum levels), vacuum level, and number of cycles [30].

CubeSat	Model	T max (°C)	T min (°C)	Vacuum level (torr)	Number of cycle
QB50	Proto flight	+50	-20	7.5×10^{-6}	4
Step Cube Lab	Flight	+35	-35	$<10^{-5}$	2
AAU CubeSat	Flight	+85	-10	<0.01	1
Swiss Cube	Flight	+50	-45	10^{-5}	4
NanoSact-BR1	Flight	+50	-10	3.75×10^{-6}	2
SERPENS	Flight	+42	-15	3.75×10^{-6}	3

pressure of 4.0×10^{-2} torr. This vacuum value is lower than the level that could be achieved in orbit. Space vacuum involves pressures between 10^{-6} and 10^{-9} torr; for instance, satellites in LEO (Low Earth Orbit) environments could achieve vacuum values below 10^{-8} torr [31, 32]. However, considering that the Simple-2 prototype lacks an external case, their vacuum exposure is sufficient to evaluate its reliability through the statistical tests.

5.1. Positive Thermal-Vacuum Tests. The technical considerations for the thermal-vacuum cycle tests were established based on two premises: firstly, the test regulations applied to small satellites were reviewed for their qualification; also, research documents related to tests applied to CubeSat and CanSat prototypes were evaluated, as shown in Table 3.

Secondly, the installed capacity was explored in terms of locally available equipment that complied with the specifications for thermal-vacuum tests intending to define the treatments applied to the experimental units. To the previous premises, the summary of the experimental tests is explained in Table 4.

The response variables consisted of some main temperature sensors (T_1, T_2, T_3) as part of the satellite thermal monitoring system. Importantly, these tests are aimed at determining the satellite's performance and making a characterization process (response) of the variables involved for further calibration. For this, intervals of stabilization of temperature and vacuum immersion time corresponding to 1 hour were used. For these tests, two Simple-2 modules were included as experimental units, which were arranged in a thermal adapted chamber (Figure 7) where treatments A and B were applied, respectively.

Figure 8 illustrates the temperature profiles of the TVCT (Thermal-Vacuum Cycling Tests). The red line profile represents simulated or design temperature. The highlighted areas correspond to the time interval known as stabilization phase or soak time of one-hour duration, which corresponds to the typical thermal cycling profile valley. The data closest to the stabilization valley of temperature and vacuum were postprocessed and used in different statistical inference tests. Figure 8 presents the thermal-vacuum cycle profile for S2-1 and S2-2 modules, respectively.

Treatment C consisted of a simultaneous test of the two experimental units under controlled environmental conditions to gather information from a different environment to contrast the response variables.

6. Vibration Test Considerations

Mechanical stresses and vibrations experienced by a satellite during launch might cause damage to the hardware and the disconnection of modules or electronic connectors. Careful choice of the overall structure is mandatory, as well as the elements and electronic devices, their encapsulated system, and footprint on the PCB on which the solder intended to fix the components is added. Efforts must be made, in equal measure, to apply practices and techniques driven at improving the performance of connections, taking care with the use of surface mount devices such as BGA (Ball Grid Array), which are more sensitive to vibrations [12].

The vibration tests present in the standard ISO-17770:2017 for small satellite modules include random vibration and shock tests and qualitative and visual inspections. The conditions established for each of these tests vary and depend on the type of launcher hired since each rocket and its deployment system have different minimum requirements [38].

To advance, in the certification process for the launch of the Simple-2 modules, vibration tests were performed using a shaker to excite the structure in its transversal axis and specific frequency ranges.

6.1. Transient Shock Test. Shocks or impacts may occur due to the application or sudden release of loads associated with CubeSat deployment or separation and possible impacts. In such events, explosives are usually used that generate particular characterized environments by high-frequency changes in acceleration, which typically decay between 5 and 15

Table 3: Some references of qualification test regulations for CubeSat satellite systems, their common vacuum levels, and number of cycles.

Type	Norm	Vacuum level (torr)	Number of cycle	Reference
Qualification	GSFC-STD-7000	10^{-5}	24	[33]
	MIL-HDBK-340A	10^{-4}	6	[34]
	ECSS-E-ST-10-03C	7×10^{-6}	—	[35]
	TR-2004 (8583)-1 Rev.A	10^{-4}	6	[36]
	NASA LSP-REQ-317.01 Rev.B	10^{-4}	1	[37]

Table 4: Detail of the treatments applied to experimental units, the stabilization cycles, and the response variables.

Experimental unit	Treatments	Cycle time (stabilization)	Responsible variables
S2-1	A (+30°C @4.0×10^{-2} torr) B (+45°C @4.0×10^{-2} torr) C (+22°C @637.55 torr)	1 h	T_1S_1, T_2S_1, T_3S_1
S2-2			T_1S_2, T_2S_2, T_3S_2

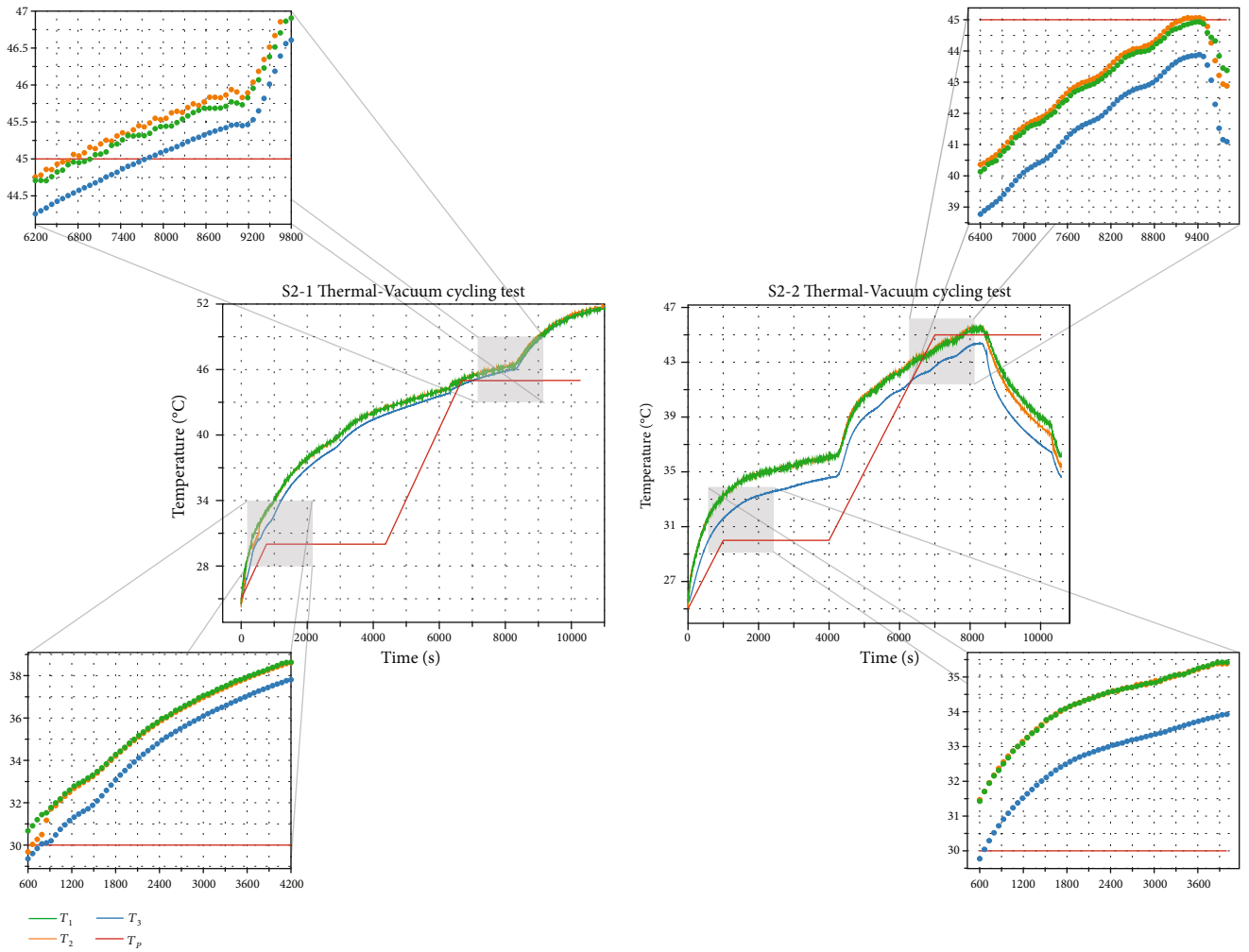

Figure 8: TVCT profiles of the units S2-1 and S2-2, corresponding to A and B treatments. The green, blue, and orange lines correspond to recordings to the sensors T_1, T_2, and T_3, specified in Table 1.

milliseconds. One of the interests in the subject of vibration consists of searching for resonances at specific frequencies, which generate abrupt exchanges of different energies for some high frequencies. There, dynamics appear that show unpredictable ranges of operation where the probability of failure increases [39].

6.2. Sinusoidal Vibration Test. The sinusoidal vibration test is necessary to perform on small satellite devices due to the periodic excitations caused by rotating elements, for example, motors, pogo-type instabilities (structural interaction and propulsion dynamics), and flutter (structural dynamic and aerodynamic interactions), combustion instability during the vehicle launch or transportation [40]. Sinusoidal vibration test and vibration waveforms were applied to a range of frequencies for which the amplitude and frequency of these waveforms are considered discrete at any instant of time. For a given acceleration, the displacement increases as the frequency decreases; that is why, at low frequencies, the displacement could exceed the equipment's limits under test. Some specifications of this kind of test use displacement for the amplitude in the low-frequency range. Usually, a frequency range between 20 and 2000 Hz is advised [39].

6.3. Oscillation Test. Following the standard ISO-17770:2017, the recommended tests were carried out, and the oscillation tests were also performed, which consisted of making the experimental units oscillate in two different configurations illustrated in Figure 9. In them, the length ($L_1 = 600$ mm and $L_2 = 450$ mm) of the radius of oscillation was changed. The frequencies of the accelerations excited by the movement of the pendulum are in the measurable range by the IMU, below 5 Hz. This kind of test was carried out to obtain comparison ranges of the dynamics perceived by both the reference accelerometer and the instruments of the Simple-2 module.

Another argument for testing the modules under these kinds of scenarios is their operation as the main payload of high-altitude balloons, since during the ascent of these, oscillations are experienced while the payload is suspended by means of ties.

7. Results

7.1. Results of Thermal-Vacuum Tests. In obtaining a dataset of the response variables, it was necessary to determine if their variability corresponded to each of the treatments applied. In the first place, it was intended to implement a one-way ANOVA. However, checking each one of the model assumptions, it was determined that the data did not follow a normal distribution by the Kolmogorov-Smirnov test (P value = 0), disabling this analysis.

Because the assumption of homoscedasticity via Levene's test assumes that each group has the same variance, the nonparametric test of Kruskal-Wallis was used to determine if each of the data samples came from the same population (distribution). In this particular case, this test was used to determine whether the measurements corresponded or not to the applied treatments. The Kruskal-Wallis test determined that there were differences in at least two response variables with an average P value ≈ 0 with respect to a significance level of $\alpha = 0.05$. A nonparametric inference was made to compare multivariable data samples for one factor with multiple responses to corroborate previous analysis. Table 5 shows the results of three multivariate statistics: ANOVA-type test, McKeon approximation for the Lawley-Hotelling Test (LH Test), and Wilk's lambda test, from which the null hypothesis of equality of mean vectors was rejected with a confidence level of 95%.

Like the one-way ANOVA, the Kruskal-Wallis test determined differences in each of the answers but did not specify which ones. For this, it was necessary to apply a nonparametric *post hoc* test that was adjusted to the absence of normality to find out the groups in which there were significant differences. The Tukey HSD (Honestly Significant Difference) test was used, and three groups were found that corresponded to the three applied treatments. However, to know the effect size and the significance between sample pairs, in this case, between the measurements of the sensors of each experimental unit, the MWW test (Mann-Whitney-Wilcoxon), also known as Wilcoxon rank-sum test, was implemented like homolog to the t-test for the parametric cases [41]. Figure 10 shows the results of both the multiple-range test and the Wilcoxon comparison test. Thanks to this, the experimental units 1 and 2 had similar behavior in terms of similarities present in sensors T_1 and T_2 in comparison with sensor T_3.

To compare the temperature sensor readings of the experimental units per treatment and the accuracy indicated by the manufacturer, confidence intervals were estimated for the standard deviation with a chi-square distribution. The results of these estimates can be seen in Table 6.

It is important to note that during treatment A, the sensor T_1S_1 increased its uncertainty by 31% equivalent to ±0.626525°C concerning the datasheet information submitted by the manufacturer. During treatment A, both the sensor T_3S_1 and the T_3S_2 showed an average increase of 46% equivalent to ±0.93534°C in their uncertainty in comparison with the manufacturer's references. For treatment B, the sensors T_3S_1 and T_3S_2, of both experimental units, increased their uncertainty by 4.4% (±0.0882864°C) and 40.4% (±0.809163°C), respectively. The other sensors kept their uncertainty below the levels indicated by the manufacturers. The above was also maintained in the two experimental units during treatment C.

The boxplot diagram of Figure 11 allowed to graphically relate the response of each experimental unit and its standard deviations (variability) for each applied treatment, according to the previous estimate for the confidence intervals. Additionally, it was possible to notice that the measurements of both experimental units during treatment B presented, in general terms, greater precision and greater accuracy with some deviations for the sensors T_3S_1 and T_3S_2. According to the results of treatment A, it was inferred that both modules were quite sensitive to increases because, their uncertainty at +30°C, given that the measurements were neither accurate nor precise. The above can see in deviations of the sensors T_1S_1, T_3S_1, and T_3S_2 and may be due to fluctuations in the thermal-vacuum

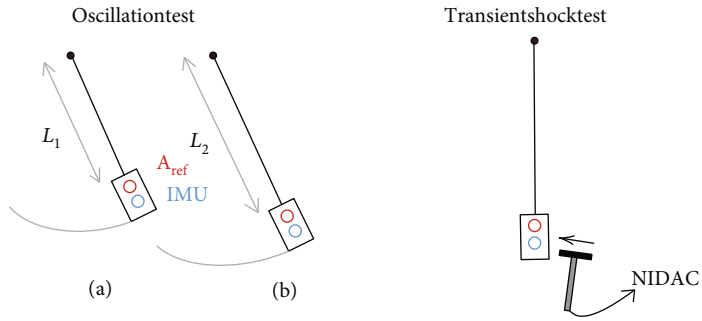

Figure 9: Schematic of the oscillation and transient shock tests.

Table 5: Nonparametric inference results for the comparison of multivariate data samples.

NPMV test	Test statistic	df_1	df_2	P value	P.T. P value
ANOVA type test P value	13654.33	2	51917.94	0	0
LH test	14340.41	2	51933.00	0	0
Wilk's lambda	14340.41	2	51933.00	0	0

chamber stabilization at that reference temperature. Concerning treatment C, it was possible to determine that the different sensors' responses were kept below the uncertainty levels and were quite precise and slightly accurate. However, like treatment A, the presence of outliers was due to the nonlinear behavior in stabilizing temperature. Experimental unit S2-2 was selected from the previous studies as a reference for data analysis during the flight test.

7.2. Results of Vibration Tests. For the measurements, a piezoelectric accelerometer of reference A_{ref} of 3 axes (PCB PIEZOTRONICS 356A01) was implemented. It was then connected to an NI 9233 acquisition module of four channels sampled simultaneously at 24-bit resolution and equipped with antialiasing filters through an interface developed in LabView. Between 3 and 70 captures were made in each test to carry out postprocessing of the data to generate a better statistical representation of the dynamic behavior.

The data with errors such as peaks in the signals generated by the test equipment were discarded. The remaining data were smoothed using the average of the samples, and the units were converted to gravities (g). These units were chosen for two reasons: the calibration parameters of the instruments related to millivolts measured in gravities and because of their widespread use in the reference literature [42, 43]. The final data were obtained by averaging the analyses in each run, revealing the expected responses, and reducing the stochastic behaviors. The vibration tests carried out (shock, oscillation, sinusoidal) allowed to determine characteristics in the dynamic responses of the module [43]. The MEMS (Microelectronic Mechanical System) accelerometer integrated into the modules was characterized and calibrated.

7.2.1. Transient Shock Test. This test led to identifying the module's resonant modes when excited in a wide band of frequencies by an impact (Dirac). Faced with this stimulus, the data delivered by the accelerometer allowed identifying which frequencies were amplified and which frequencies attenuated.

Figure 12 shows the response in the frequency domain of the accelerometers in each of the axes. Figure 12(a) of test A shows the result of the impact on the structural case manufactured by 3D printing in ABS (Acrylonitrile Butadiene Styrene) that covered the battery. Figure 12(b) of test B corresponds to the results of the impact generated in one of the bronze standoffs between the PCBs. Although a wide band of frequencies was stimulated, according to the hammer (violet) response, it was confirmed that the highest confidence results were up to 1000 Hz.

The prominences located between 15 and 35 Hz were not conclusive, and this can be attributed to the assembly behavior used for this test. Such low frequencies could be due to mechanical looseness and not to a rigid part such as the ABS case of the Simple-2 module. Additionally, it was observed that the module amplified at least 1.4 dB in frequencies between 20 and 500 Hz for X and Y axes, which formed the plane where most of the impact was applied. Finally, it may be affirmed that the response of the module began to be relevant and triaxially coherent from 700 Hz, maximizing between 800 and 900 Hz.

It is advisable to perform tests for wide ranges so that both the frequencies required by the launcher and those required in the operation and transport of the module (workmanship forces) are sheltered [44].

7.2.2. Oscillation Test. Figures 13(a) and 13(b) correspond to the spectral representations of the dynamic responses of the S2-1 modules and S2-2 with string length L_1. Figures 13(c) and 13(d) correspond, respectively, to the same representation for the modules with string length L_2. These results showed similar frequencies of response in the four tests. These results indicated that the IMU responded consistently with the reference accelerometer at low frequencies, limited by its low resolution, given the reduced sampling rate [43]. It was also possible to perceive the difference in measurement ranges of the sensors used because the modules' IMU presented a smaller band of magnitude.

In Figures 13(a) and 13(b), it was possible to see a predominant peak at 1.33 Hz, corresponding to the oscillation frequency of the pendulum resulting from the assembly, in

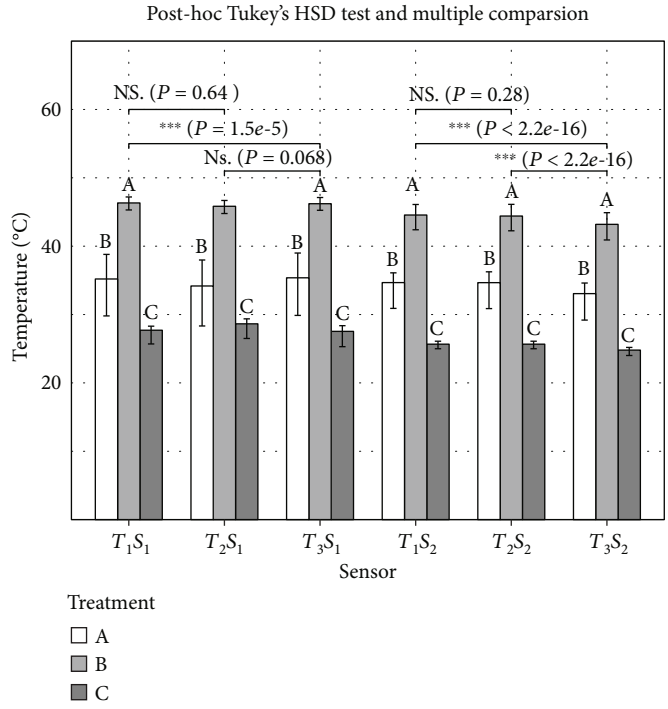

Figure 10: Post hoc Tukey's HSD test and Wilcoxon pair comparison results by treatments.

this case, for the length L_1. It is emphasized that, for modules, both S2-1 and S2-2, the detected peak frequency was equal to 1.33 Hz. In Figures 13(c) and 13(d), it was found that the results of the length L_2 are corresponding with a peak frequency of 1.46 Hz. It is also possible to note that the frequencies at around 7-10 Hz correspond to the experimental setup accessories.

To measure similarities between the IMU and reference accelerometer, each signal was correlated with itself to extract their periods, using Matlab. These periods were compared, calculating their difference in seconds and then comparing their difference in respect to the captured signals, as shown in Table 7. The above validated the capacity of the Simple-2 module to measure low frequencies, since the differences between the period measured by the reference accelerometer and the IMU were small, bearing in mind that the time between samples or module sampling period was 0.1217 s. These phase differences (lags) correspond to an error of 3.9% with respect to the period, equivalent to differences in response times of 0.53% for L_1 and 4.1% for L_2. These results are consistent given that the shorter the period, the greater the lags in response time.

7.2.3. Results of Sinusoidal Vibration Tests. In the sinusoidal vibration test with the Shaker Agate AT-2040 (see Figure 14), a discrete sweep was carried out from 10 Hz to 50 Hz with intervals of 10 Hz and continuing from 100 Hz ant 150 Hz to 200 Hz. It was increased up to 1500 Hz, varying the frequency changes with an interval of 100 Hz. Finally, the module was excited up to 2000 Hz with a constant excitation amplitude of 1 g_{rms}.

From this test, the frequency responses and their RMS (Root Mean Squared) and PSD (Power Spectral Density) magnitudes were extracted, as shown in Figure 15. The results showed that the satellite module's first resonance was found between 400 and 500 Hz. On the one hand, the bands where the amplitude of the response was less than 1 g_{rms} corresponded to attenuation bands. In another sense, the band where the amplitude was greater than 1 g_{rms} was the amplification region, where the first resonance of the module was located, close to 500 Hz.

To certify any device for flight, it is necessary to submit it to a wide range of frequencies to cover all those found in different stages before its start-up, including transport and launch. To its verification, tests must be specified under minimum standards of magnitude and frequency [44] so that under these stimuli, it can be guaranteed that the module does not suffer any damage.

According to Simple-2 module's mass (0.185 kg) and the standard SMC-S-016, which requires a minimum qualification level of up to 0.2 PSD given. in g^2/Hertz and range of at least 20 to 2000 Hz [45], the module was tested in this frequency range with higher constant intensity of 1 g^2/Hz. This test guaranteed the module's structural and operative integrity, which did not present detectable physical alterations or discontinuous operations. Figure 15 shows the response of the measured module with the reference accelerometer located at the top of it, revealing that the critical requencies are in an approximate range of 400 to 500 Hz.

7.3. Results of Flight Test. Two CanSat Simple-2 modules were tested as the main payload aboard a stratospheric balloon (BalloonSat) on November 5, 2017, at the coordinates

Table 6: Confidence intervals: chi-square distribution by treatments and response variables.

Treatment	T_1S_1	T_2S_1	T_3S_1	T_1S_2	T_2S_2	T_3S_2
A	$2.561220 \leq \sigma \leq 2.695273$	$2.603796 \leq \sigma \leq 2.740077$	$2.402375 \leq \sigma \leq 2.528113$	$1.247728 \leq \sigma \leq 1.313033$	$1.262443 \leq \sigma \leq 1.328519$	$1.302139 \leq \sigma \leq 1.370292$
B	$0.4826614 \leq \sigma \leq 0.5083373$	$0.5053857 \leq \sigma \leq 0.5322704$	$0.4759570 \leq \sigma \leq 0.5012762$	$1.104990 \leq \sigma \leq 1.163771$	$1.110933 \leq \sigma \leq 1.170030$	$1.178632 \leq \sigma \leq 1.241331$
C	$0.5227104 \leq \sigma \leq 0.5506271$	$0.5431524 \leq \sigma \leq 0.5721609$	$0.5509851 \leq \sigma \leq 0.5804118$	$0.2092442 \leq \sigma \leq 0.2204194$	$0.2092442 \leq \sigma \leq 0.2204194$	$0.2049021 \leq \sigma \leq 0.2158454$

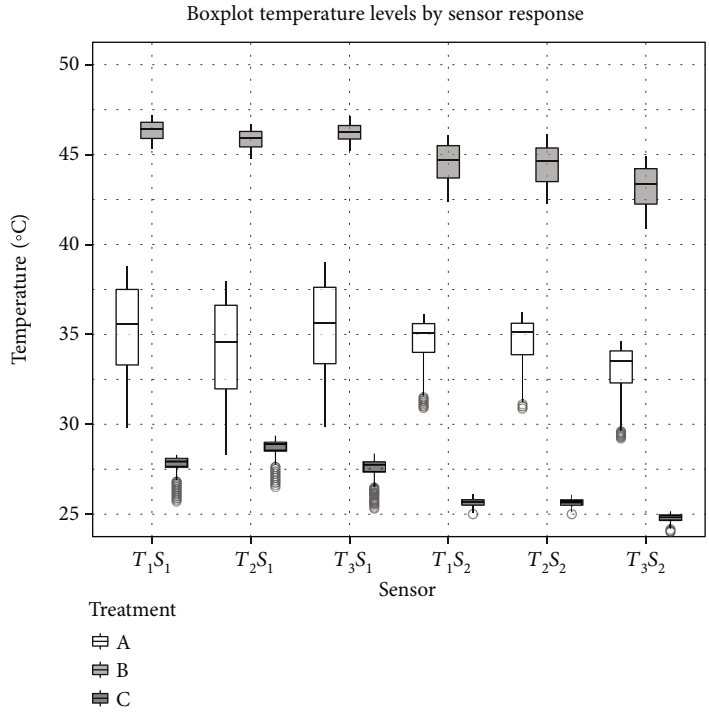

Figure 11: Boxplot temperature levels by sensor response per treatments.

5.4745984°N, -74.6603083°W. The S2-1 module was placed inside a stratospheric sonde while the S2-2 was transported as peripheral, as shown in Figure 16. It is also possible to observe the GPS trajectory in both the internally and externally located devices in the ascent vehicle.

The mission statement was to estimate the variability, with respect to the change in the altitude of thermodynamic variables (described in the one-factor experiments) and to measure the concentrations of some gases species. The device was recovered at the coordinates 5.4961331°N, -74.7296626°W) after a total flight time of 01:12:00.

Some of the data collected during the external module's flight showed its variation in respect to the time in Figure 17. Figure 17(a) shows the altitude change as the device ascends to the apogee or maximum altitude reached by the sonde. In Figures 17(b)–17(d), it can be seen how the values of relative humidity, temperature, and barometric pressure decay during the total ascent time. It is important to note in Figure 17(c) the inflection point at 12:56:04 (UTC), which demarcates the transition region between the troposphere and the stratosphere. In the tropic, this region is around 17 km, where there is a sudden increase in temperature due to the interaction of ozone with ultraviolet rays from the sun.

It is noteworthy that, from all the data captured during the sonde's total flight time, only the data from the ascent stage were used for the statistical tests because, during the descent stage, the sonde experienced higher speed with respect to the ascent, which caused few samples in that acquisition period. This reduction in the number of samples during the descent did not guarantee the determination of the sensor output signal's hysteresis or deviation at a specific point of the input signal.

For flight data analysis, physical quantities T_1, T_2, T_3, P, and RH and gas concentration (in parts per million (ppm)) of the CO, NO_2, C_2H_6OH, H_2, NH_3, CH_4, C_3H_8 and C_4H_{10} were conceptualized as DV of the IV (independent variable) A_1 (GSP altitude). It should be noted that the variable A_2 was not considered for this study, given that it is a measurement dependent on barometric pressure. Additionally, a confidence interval was estimated for the variance of the F test between A_1 and A_2. The result of Equation (1) shows that the uncertainty of the sensor A_2 was increased by 31%, while the nominal value of the sensor accuracy A_1 remained below the calculated interval.

$$1.069884 \leq \sigma \leq 1.189693. \quad (1)$$

A correlation matrix was constructed to determine the relationship intensity between DV and IV. It should be noted that, on an experimental level, the correlation is usually used when none of the variables has been controlled; it has just been measured to find out if they are related or not [46].

As a selection criterion, the variables whose correlation coefficient or effect size was between ±0.7 (high association) and ±0.9 (very high association) was considered. Therefore, the variables corresponding to C_2H_6OH, CH_4, C_3H_8, and C_4H_{10} were discarded as can be seen in Figure 18. It is observed that the majority of correlation coefficients, according to the selection criteria, have a highly negative relationship (high negative correlation), which will be reflected in the selected regression model.

Then, a regression analysis was conducted using simple linear models to adjust a model to the data. The regression coefficients were estimated from the observations, and the

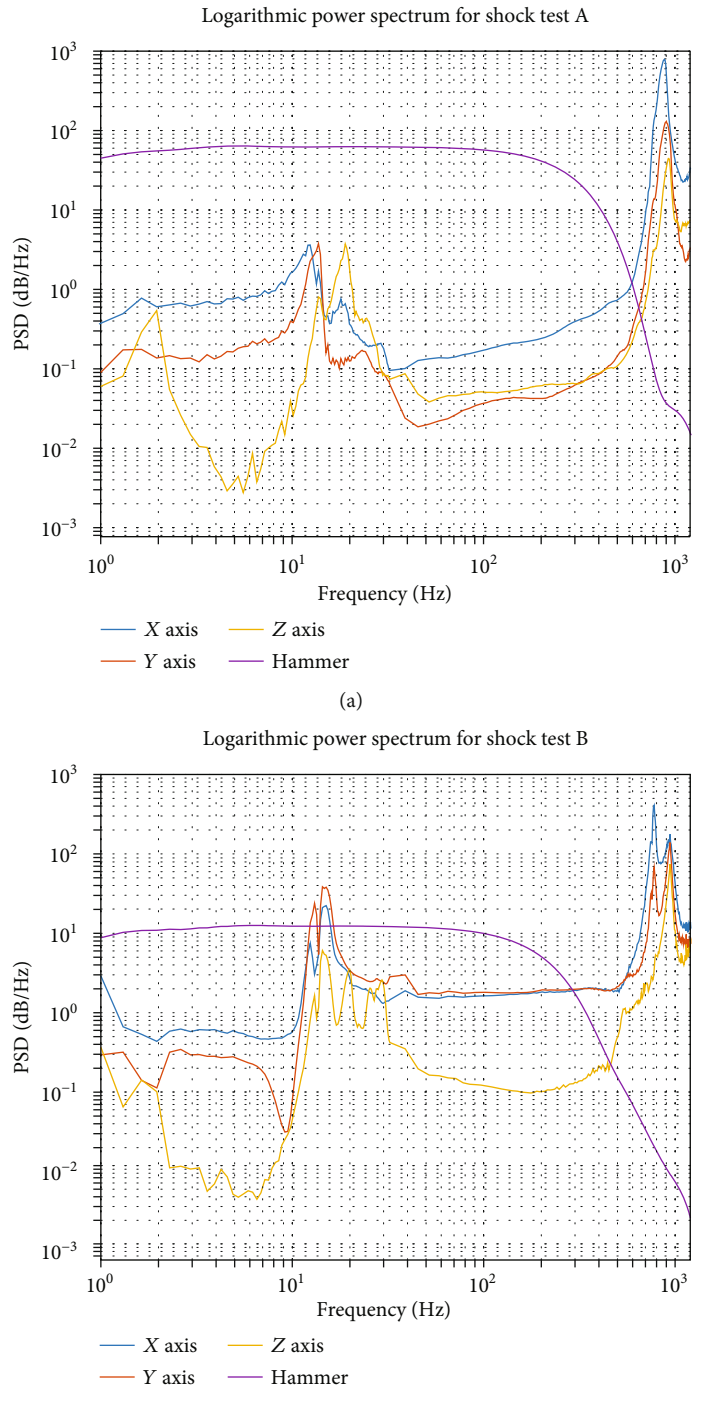

Figure 12: Frequency response for shock test.

response variables or DV were predicted, given its relationship with altitude as a quantitative predictor variable. A diagnosis was made of the assumptions of this model (simple or multiple) in terms of linearity, homoscedasticity, normality, and independence of errors or residuals. An adequate one-line summary of the linear model (implicit independence) is presented in Equation (2) [47]:

$$Y \mid \left(X_1 = x_1, \cdots, X_p = x_p\right) \sim \mathcal{N}\left(\beta_0 + \beta_1 x_1 + \cdots + \beta_p x_p, \sigma^2\right). \tag{2}$$

A graphical diagnosis of the residuals versus the predicted values was made. Similarly, the normal quantile-quantile plot was obtained. In both, the presence of linearity

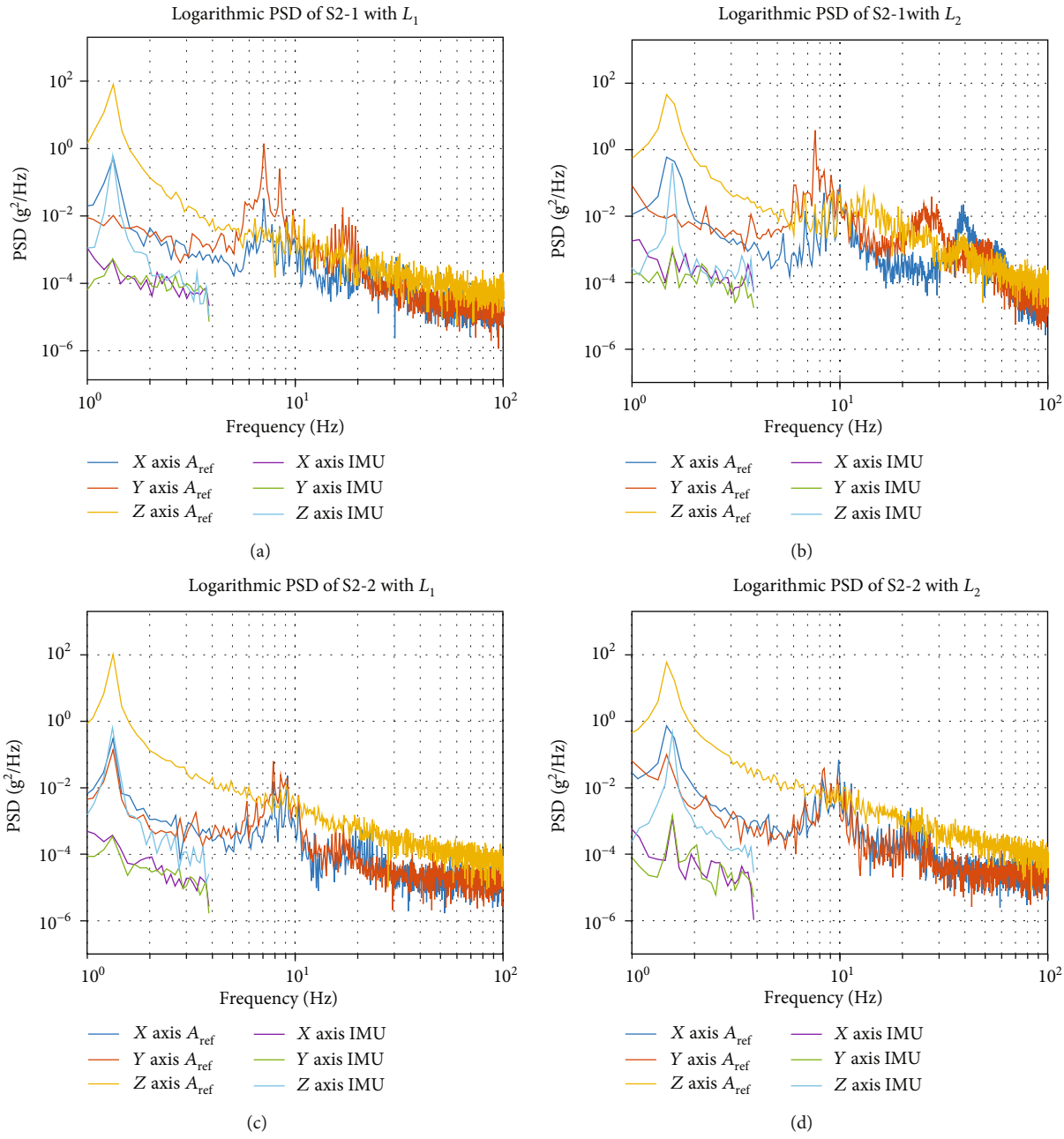

Figure 13: Frequency response for the oscillation tests in the two experimental units with the lengths L_1 and L_2.

Table 7: Estimated errors of the IMU using cross-correlation.

Length	S2-1				S2-2			
	IMU (s)	A_{ref} [s]	Dif (s)	% error	IMU (s)	A_{ref} (s)	Dif (s)	% error
L_1	0.7606	0.77	0.0094	1.2326	0.7606	0.7647	0.0041	0.5376
L_2	0.6338	0.6567	0.0229	3.543	0.6338	0.6607	0.0269	4.1501

and homoscedasticity in the residuals could be appreciated. Nevertheless, the assumptions of normality and independence were not satisfied. Given the above, the normality hypothesis tests of Shapiro-Wilks and Kolmogorov-Smirnov ($n > 30$), the independence of the residuals of Durbin-Watson, and the Levene test were performed. Only the latter was met since the P-value exceeded the significance level of$\alpha = 0.05$, and it was not possible to reject the null hypothesis because variances are homogeneous.

According to the previous information, outliers were removed to rule out the possibility that these were the potential causes of noncompliance of the assumptions. Although

Figure 14: Simple-2 module installation detail in the AT-2040 Agate Shaker for sinusoidal vibration test.

the P values of the statistical tests improved, they did not exceed the level of significance.

The remaining option was the transformation of the data to achieve its adaptation to the simple linear model. For this, the simple power transformation of Yeo-Johnson was implemented. This is a variation of the Box-Cox transformations, where the dependent variable Y does not have to be strictly positive; it accepts negative values and equal to zero, as in the variables of the implemented dataset. This transformation was aimed at finding values for the power (λ) to improve the distribution of the residuals, the inequality in the variances, and the nonlinearity between the DV and IV. Once lambda values for each of the DVs were determined, these were replaced in each of the linear models. Given that noncompliance of assumptions continued to prevail, nonparametric regressions were formulated.

7.3.1. Nonparametric Regressions. The previous study revealed no linear relationship between the responses (DV) and the predictor (IV) of the dataset. The nonparametric test of Kruskal-Wallis was executed to check this hypothesis. The results show an average P value of 0.48, so there is enough evidence to not reject H_0. It can be affirmed then that there are no differences between the medians' observations in the different measurements. Kruskal-Wallis indicated that linear regression is not adequate to analyze the dataset.

After recognizing that the data presented a nonlinear distribution, it was necessary to review the correlation coefficients obtained in Figure 18. Although these coefficients were obtained by the Pearson method whose values are fairly robust despite the lack of normality [48], these are sensitive to extreme values, so it is recommended to use the Spearman correlation as a nonparametric method, when the normality condition for continuous variables is not satisfied nor can the data be transformed into ranges. In addition, the significance was calculated to confirm that there really was a relationship between each of the DVs compared to the IV. For the case of the variables A_1 and T_1 ($\rho = -0.9658884$, P value ≈ 0), it was determined that their relationship is significant.

Table 8 summarizes the application of the methods previously described in Section 3 to characterize the behavior of $T_1$with respect toA_1, the model fit criteria, and the selection among them. It is relevant to mention that these models were applied to each dataset variable, but only the results of the variables specified above will be shown for practical effects.

About to the selection criteria of the appropriate regression method to be implemented, one whose model would show the lowest MSE (Mean Squared Error) and RMSE (Relative Mean Squared Error) and a high coefficient of determination R^2 was sought out since this would provide a better explanation of the variability of the data. According to the results tabulated in Table 8, it was observed that the MSE, RMSEA, and R^2 are relatively constant in the different applied methods. For instance, the polynomial regression presented a high R^2 (-0.8725445) and slightly higher values of MSE and RMSE compared with the rest of the methods. Despite the preceding, other selection criteria could not be ignored. For example, the high computational cost of the regression methods by splines, smoothing splines, and local polynomial regression. The high degree of freedom and sensitivity to overfitting such models present when the smoothing parameter depends on small values in the bandwidth h causing greater flexibility to the estimator and high associated prediction errors [53, 55].

In Figure 19, the differences between the different nonparametric regression methods applied to the change in temperature T_1 with respect to altitude A_1 can be graphically appreciated. Note that the bandwidth of the regressions is almost imperceptible, indicating that confidence intervals are fairly accurate.

It can be seen that the polynomial regression of Figure 19(b) offers a flexible model with lower computational cost in comparison with the other methods. As mentioned above, to avoid over fittings and high polynomial degrees, this selection was made through the LOOCV (leave one out cross-validation) and one-way ANOVA with a different order of a polynomial. Additionally, although it uses local regressions in each kernel in function domain, the local polynomial regression method was implemented as a graphical method to validate the degree of a polynomial of the polynomial regression, as shown in Figure 19(f). The model obtained from this method, which meets the selection criteria and allows the explanation of the response variable, is shown in the following equation:

$$T_1 = -2.073 - 693.963A_1 + 168.799{A_1}^2 + 89.635{A_1}^3. \quad (3)$$

The polynomial regression method prevailed in explaining of the variability experienced by the different DVs during the ascent flight to the stratosphere. Table 9 summarizes the different regressions obtained through this method:

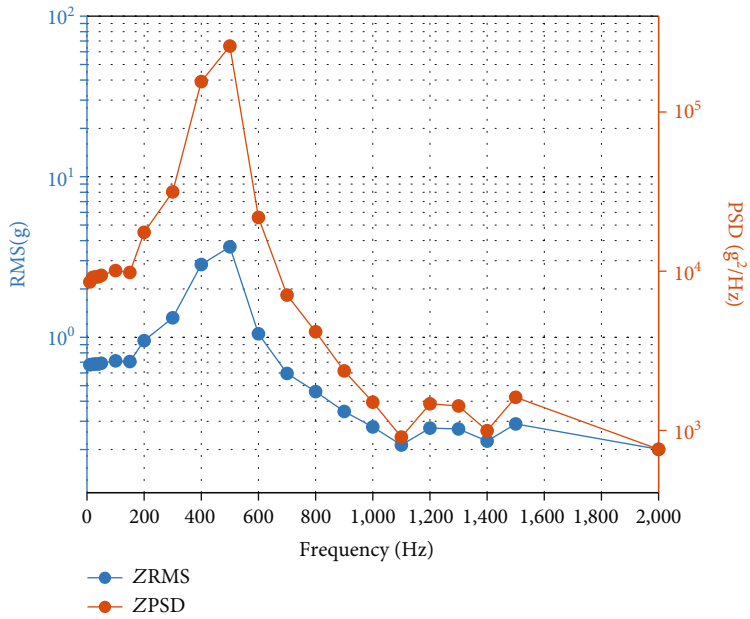

Figure 15: RMS and PSD amplitude for sinusoidal test. Lateral acceleration at the top of Simple-2 satellite.

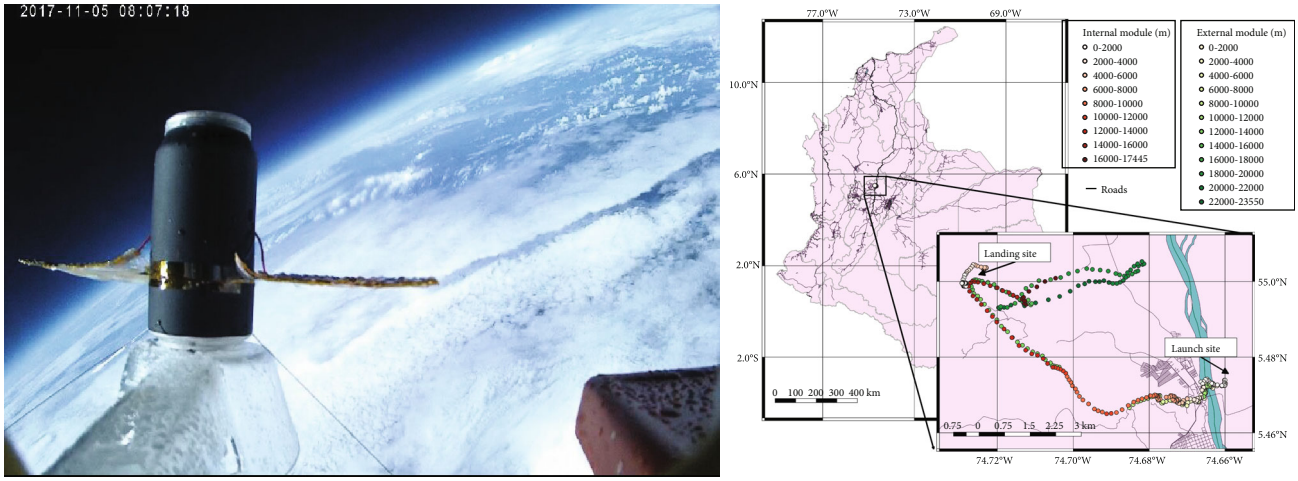

Figure 16: External CanSat S2-2 in the stratosphere just before the descent and location of the launching and splashdown site of the high-altitude balloon.

These results enabled similarities to be established between the models of the variables T_1 and T_2, given that the values of the factors (effects, regression coefficients, or slope) and intercepts of both regressions presented similar magnitudes. For example, both slopes are negative, as are their intercepts, which confirmed that the temperature decreased during altitude increase. This behavior continued to prevail in the variable T_3, even though its intercept and first slope are below the others. In general terms, these polynomial regressions facilitated the description of the decreasing behavior of the variables T_1, T_2, and T_3 as well as the variables P, RH, and NH_3. The variable NO_2 presented, on the contrary, an increasing behavior in its values as evidenced by its positive slope.

About the variables, H_2 and CO, the degrees of the polynomials used to describe the behavior of their variability with respect to the change in altitude did not provide a significant response, given that by using high degrees of the polynomial, highly flexible fits were obtained. This allowed establishing the high scattering of these agents in the first layers of the atmosphere and the low resolution of the sensor implemented for the measurement of these variables, as well as the tendency to decrease their concentrations with the change in altitude.

8. Discussion

8.1. Vibration Tests. One of the vibration tests performed was the shock test; this test's advantage was its simplicity since it

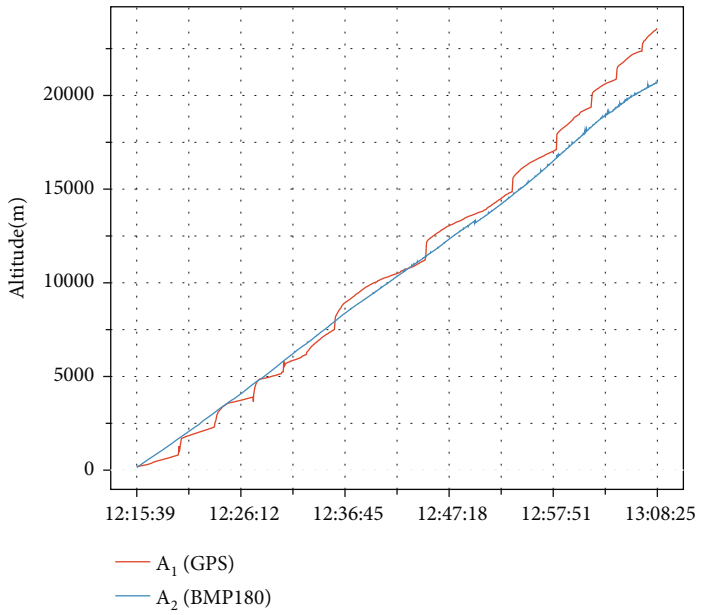

(a) Vertical altitude profiles

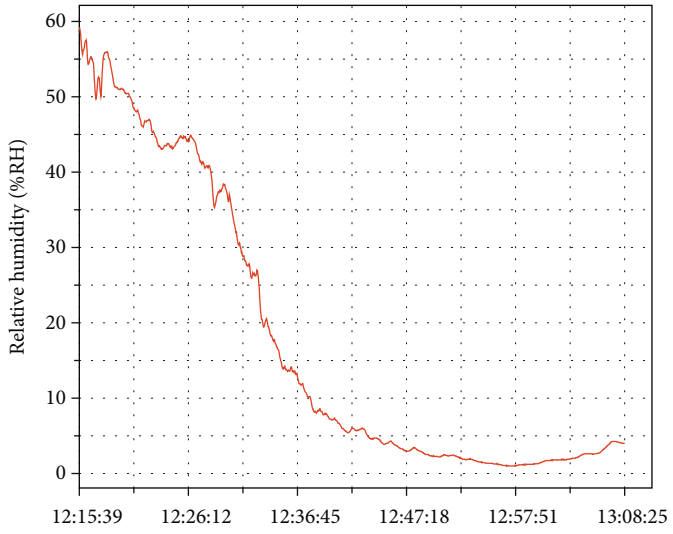

(b) Atmospheric relative humidity profile

Figure 17: Continued.

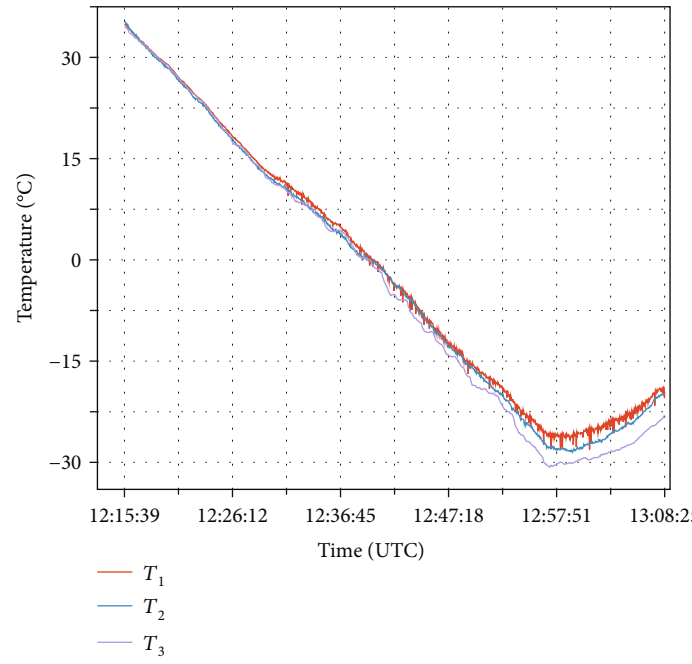

(c) Temperature readings over ascent time

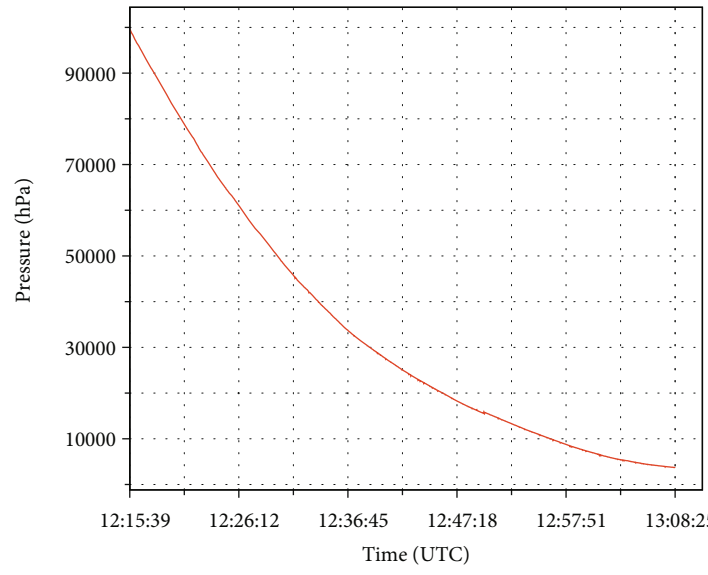

(d) Barometric pressure profile

Figure 17: Readings of different variables of the S2-2 module as a function of the ascent time of the high-altitude balloon until its apogee.

does not need a complex assembly or does not restrict the excitation under certain conditions. On the other hand, the resolution in frequency is limited only by the dynamic range of the sensors and the acquisition system. However, this test has disadvantages for the sinusoidal since the former is more laborious, concerning the repetitions to which the model must submit; it is also sensitive to the rigidity, the damping of the tip of the hammer, and the supports used. Therefore, it depends on the skill of the technician and his ability to filter the acquired data. The repetitions to which the module must be subjected to in the shock test are justified to attenuate errors derived from the assembly or inaccuracies of magnitude or location of the impact that could be the cause of the differences found in the system responses: ~900 Hz in the impact test and ~500 Hz (Figure 13) in the sinusoidal test.

Sinusoidal testing offers more controlled conditions, with a single rigid assembly and less uncertainty at discrete frequencies. In contrast, it requires more sophisticated equipment, and the excitation can be considered uniaxial, while the shock test is triaxial. In addition to the above, the same assembly required the addition of mechanical fastening elements that increased the mass of the system (0.035 kg), which

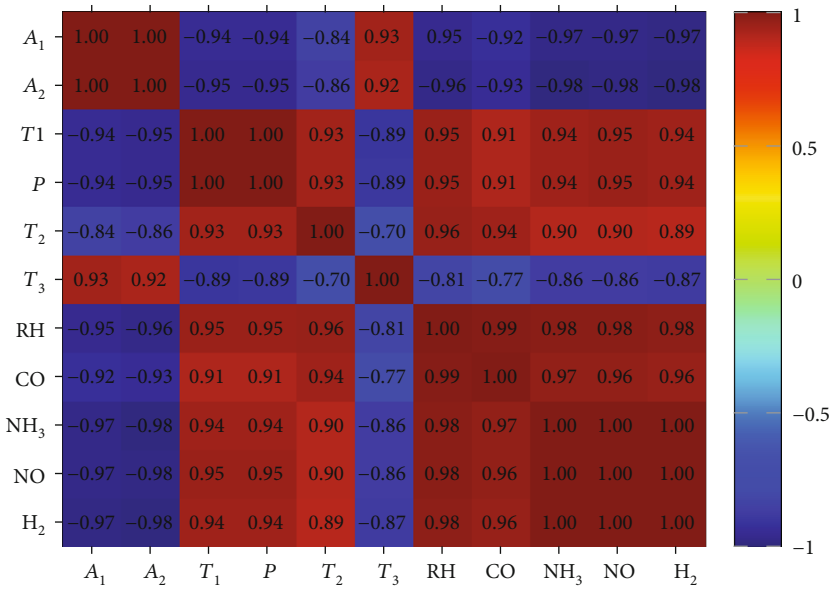

Figure 18: Correlation matrix between dependent variables DV and the independent variable IV A_1.

is attributed to a significant decrease in the dynamic responses obtained for the other tests.

8.2. Thermal-Vacuum Tests. Although for the vibration tests it was sufficient to have an experimental unit, the thermal-vacuum tests require additional units that allow the experiment's repeatability to increase its certainty (decrease the variance) and reduce the measurement errors associated with random or uncontrolled causes. The thermal-vacuum test demonstrated the Simple-2 unit operational stability and the capacity for the correct operation of all its subsystems in this kind of environment. Also, the absence of defects in the manufacturing processes and the quality of the materials used were verified. Mainly, ABS was used to manufacture the module's battery case employing additive manufacturing or 3D printing. The finish of these pieces is highly porous, which causes the accumulation of moisture. Although this additional humidity slows down the stabilization of the target vacuum pressure, it is not advisable to preheat the experimental modules since this considerably affects the thermal profiles and the soak times.

Even though the TVCT were carried out with equipment susceptible to improvements concerning the applied treatments' stability, these were reproducible and replicable, as indicated by the results obtained in Figure 10. From this, it can be inferred that both modules presented the same behavior and do not differ significantly in their responses. Furthermore, it is important to note that the thermal-vacuum chamber's differences or instabilities may be because there is not enough evidence to reject the temperature's Gaussian behavior, as shown in Figure 11.

8.3. Flight Test. In relation to the analysis of the data obtained from the flight test, the unit's operation in extreme environments could be corroborated. Figure 17 shows the data obtained during the flight, in which an inverse relationship of altitude with temperature and atmospheric pressure can be inferred, results that were expected and that demonstrate correct sensor behavior of the unit. These relationships between the variables can also be seen in Figure 18, where the correlation matrix shows a high relationship between the variables recorded by the unit, all of which are meteorological variables and gases (aerosol concentrations). It should be noted that the Simple-2 unit managed to communicate throughout the flight and sent the information during it. This concludes that all the modules that make up the unit functioned adequately despite the low temperatures reached or the low-atmospheric pressure observed in Figures 17(c) and 17(d), respectively.

This study corroborated that nonparametric regression methods are predominant tools for modeling the variability of gas concentrations and thermodynamic variables, especially when their acquisition is subject to periods of atmospheric instability. These variables presented behaviors that make it difficult to use parametric regression methods. Other studies revealed that these methods do not take into account climatological factors such as temperature, wind speed, or precipitation, which could eventually alter the typical behavior of different pollutants [56, 57]. In relation to the measurement of pollutants, although the gas sensor behaved adequately for the majority of references, it presented a high uncertainty for CO and H_2 and a low resolution in the concentrations of C_2H_6OH, CH_4, C_3H_8, and C_4H_{10}, presumably because those compounds are not very abundant in the upper atmosphere. Future developments focused on these measurements; it is proposed to use at least two sensors of this type embedded in PCB and generate a self-calibration routine that allows the corroboration of measurements between both.

8.4. Future Considerations. The results of the different experimental considerations supported by statistic inference and the test environments suggest recommendations for the

Table 8: Nonparametric regression method comparison for model selection between T_1 and A_1 variables.

Method	Model equation	Validation	Grade	Df	MSE	RMSE	R^2	References
Polynomial regression	$y_i = \beta_0 + \beta_1 x_i + \beta_2 x_i^2 + \beta_3 x_i^3 + \cdots + \beta_d x_i^d + \varepsilon_i$	Leave one out cross-validation (LOOCV) $\mathrm{CV}_{(n)} = 1/n\sum_{i=1}^{n}(\mathrm{MSE}_i)$ one-way ANOVA	3		699.7394	26.45259	-0.8725435	[49, 50]
Step functions*	$C_o(X) = I(X < c_1)$, $C_1(X) = I(c_1 \le X < c_2)$, $C_2(X) = I(c_2 \le X < c_3)$, $\vdots$ $C_{k-1}(X) = I(c_{k-1} \le X < c_k)$, $C_k(X) = I(c_k \le X)$ $y_i = \beta_0 + \beta_1 C_1(x_i) + \cdots + \beta_K C_K(x_i) + \varepsilon_i$	K-fold cross-validation $\mathrm{CV}_{(k)} = 1/k\sum_{i=1}^{k}(\mathrm{MSE}_i)$ $\mathrm{CV}_{(k)} = 1/k\sum_{i=1}^{k}(\mathrm{Err}_i)$	—	—	—	—	—	[49, 51, 52]
Regression splines	$y_i = \beta_0 + \beta_1 b_1(x_i) + \beta_0 + \beta_2 b_2(x_i) + \cdots + \beta_{k+3} b_{k+3}(x_i) + \varepsilon_i$	K-fold cross-validation $\mathrm{CV}_{(k)} = \frac{1}{k}\sum_{i=1}^{k}(\mathrm{MSE}_i)$ $\mathrm{CV}_{(k)} = \frac{1}{k}\sum_{i=1}^{k}(\mathrm{Err}_i)$	2,3	4-16	698.1634	26.42278	-0.8583486	[49, 51, 52]
Smoothing splines	$\sum_{i=1}^{n}(y_i - g(x_i))^2 + \lambda\int g''(t)^2\,dt$, $df_\lambda = \sum_{i=1}^{n}\{S_\lambda\}_{ii}$	K-fold cross-validation $\mathrm{RSS}_{\mathrm{cv}}(\lambda) = \sum_{i=1}^{n}\left(y_i - g\wedge_\lambda^{(-i)}(x_i)\right)^2 = \sum_{i=1}^{n}\left[y_i - g\wedge_\lambda(x_i)/1 - \{S_\lambda\}_{ii}\right]^2$	3	92.72798	698.1634	26.42278	-0.8583486	[49, 51]
Local regression	Local linear regression (LOESS) $\widehat{f}(x_0) = \widehat{\beta}_0 + \widehat{\beta}_{1x_0} = \underset{\beta_0,\beta_1}{\operatorname{argmin}}\sum_{i=1}^{n} K_{i0}(y_i - \beta_0 - \beta_1 x_i)^2$ Local polynomial regression $\widehat{f}_{h,(x_0)} = \widehat{\beta}_{h,0}, \cdots, \widehat{\beta}_{h,p} = \underset{\beta_0,\cdots\beta_p}{\operatorname{argmin}}\sum_{i=1}^{n} K_h\left(y_i - \beta_0 - \beta_1 x_i - \cdots - \beta_p x_i^p\right)^2$	Assign weights (kernel functions)** $K_{i0} = K(x_i, x_0), s = k/n$ $K_h = K(x_i, x_0) = K\left(\frac{x_i - x_0}{h}\right)$	$s = 0.7$ $h = 0.25$		696.9988	26.40073	-0.8552487	[49, 53, 54]

*The step functions were only used for the degrees of the functions of the regression splines. ** The K function is named kernel function, and in general, it is a continuous density function, unimodal, and symmetric around 0. The parameter h is known as the smoothing parameter.

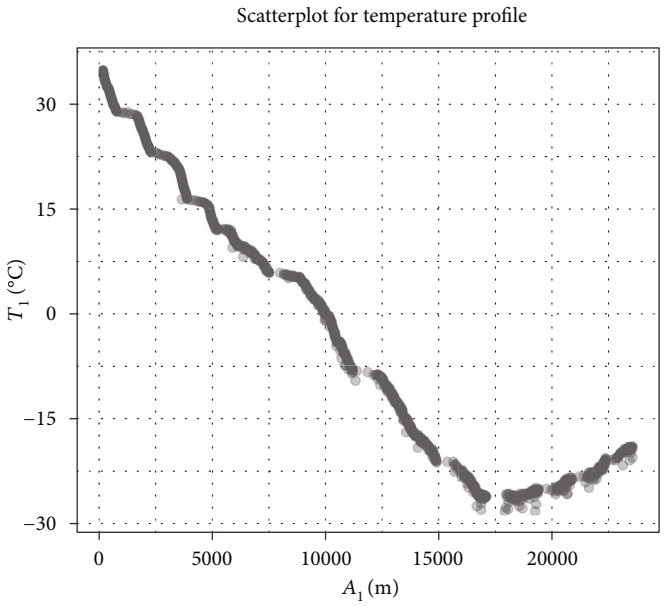

(a)

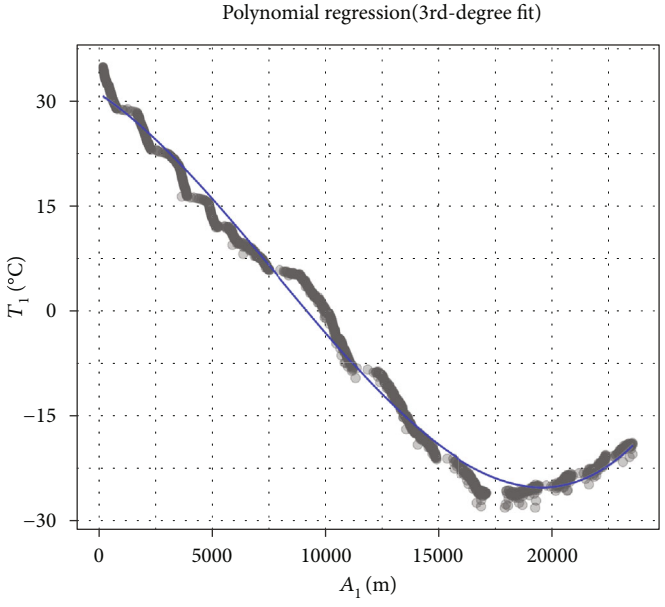

(b)

Figure 19: Continued.

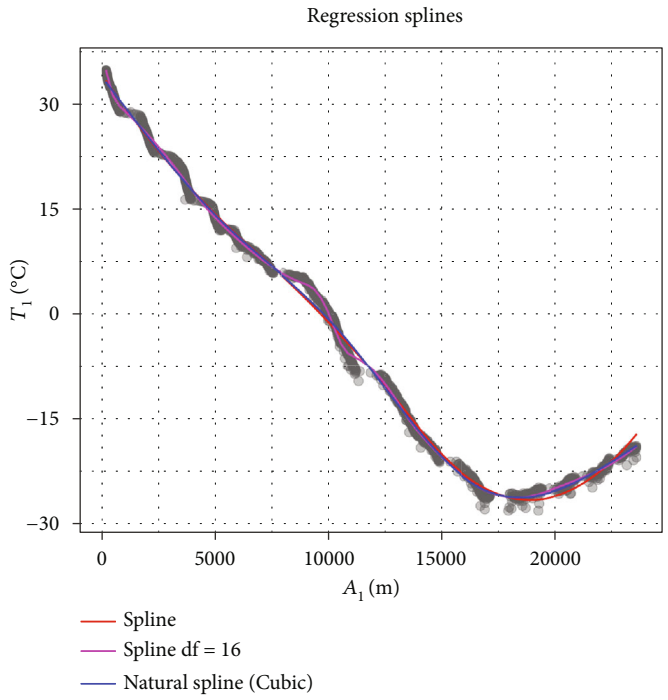

(c)

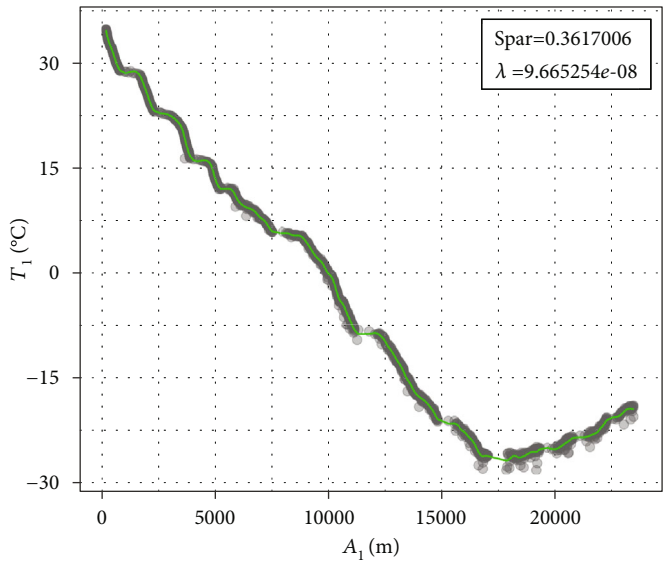

(d)

Figure 19: Continued.

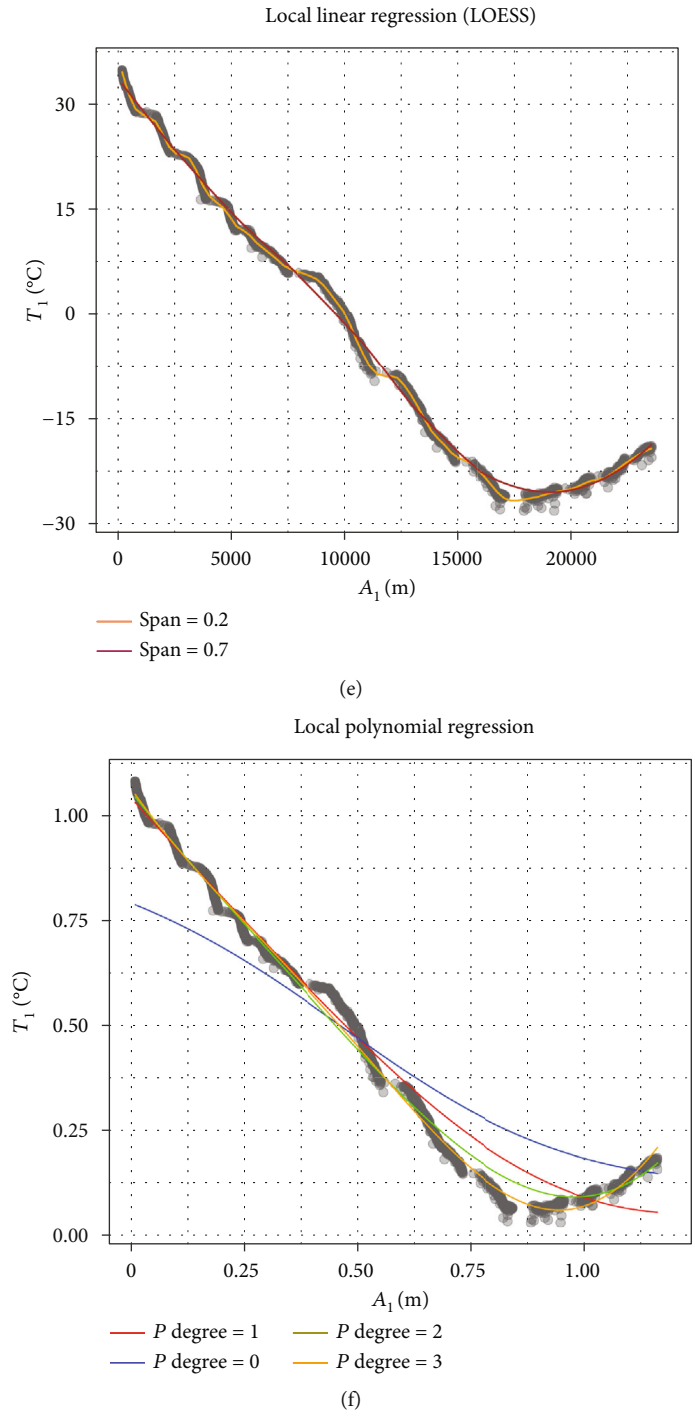

Figure 19: Estimation of different nonparametric fittings for the relationship between the variable T_1 as a function of the variable A_1.

future related to testing protocols and adaptations or redesigns in the hardware. For example, the OB&DH accelerometer needs to be updated and replaced with another one with more appropriate dynamic ranges. Although the barometer used in flight operated within the measurement ranges, the same did not happen when subjected to high vacuum conditions. Therefore, one recommendation is to use a higher resolution pressure sensor to operate in near-space conditions and even in orbital conditions. For temperature measurements, it is recommended to check both the operating ranges of the T_3 sensor and consider its relocation over PBC of the payload subsystem to avoid it being affected by external heat sources that bias its uncertainty scale. It is also advised that the T_3 sensor be mounted with slots milled into PCB to minimize heat transfer for future prototypes.

Finally, to redesign the Simple-2 module or to build future prototypes, it is essential to consider two independent PCB boards for the payload and EPS subsystems. The latter

Table 9: Local polynomial regression equations for dependent variables by the altitude rate.

Variable	Polynomial degree	Model equation	MSE	RMSE	R^2
T_2	3	$T_2 = -2.875 - 707.760A_1 + 166.051A_1^2 + 92.320A_1^3$	728.1202	26.9833	-0.855773
T_3	3	$T_3 = -3.968 - 748.028A_1 + 159.855A_1^2 + 95.934A_1^3$	802.0293	28.32012	-0.8613144
P	2	$P = 33498 - 953011A_1 + 335471A_1^2$	1316459319	36283.04	-0.8833828
RH	3	$\mathrm{RH} = 17.3787 - 630.115A_1 + 320.6150A_1^2 + 14.647A_1^3$	667.7055	25.84	-0.8553756
NO_2	3	$\mathrm{NO} = 0.597 + 15.937A_1 + 4.733A_1^2 + 1.305A_1^3$	0.3448327	0.5914665	-0.9153624
NH_3	3	$\mathrm{NH_3} = 4.068 - 25.532A_1 + 14.111A_1^2 - 7.595A_1^3$	1.25867	1.061069	-0.91263
H_2	4	$\mathrm{H_2} = 22.496 - 30.414A_1 - 2.342A_1^2 - 3.140A_1^3 + 3.733A_1^4$	1.191081	1.091367	-0.88196
CO	4	$\mathrm{CO} = 41.407 - 36.712A_1 - 3.115A_1^2 - 3.759A_1^3 + 4.503A_1^4$	1.740338	1.319219	-0.879633

with the goal to know if the electrical supply to other subsystems could be more stable, adding different filtering stages to estimate changes in consumption patterns, given the power electronics could work a natural noise source in the experiments sensitive to thermal drifts, as is shown in Figure 11 results.

9. Conclusions

With the development of this research, an experimental methodological approach was proposed to be reproduced with small satellites in the pico- (0.1-1 kg) and femto- (0.01-0.09 kg) form factor in evaluating the feasibility of using COTS components in a space project to reduce costs considerably, as well as to validate the modularity of the internal subsystems to allow reuse in the future missions. This research's main findings were (1) CanSat standards and regulations, (2) modular design methodology, (3) the technology validation, and (4) supporting documentation and structural stability. The following set of conclusions is as follows:

(1) This study demonstrated the feasibility of establishing and applying an acceptance and qualification test methodology to observe CanSat prototypes' performance through the revision, adaptation, and/or scaling of standards for the CubeSat form factor. The ability to establish these new test protocols depends largely on the availability of laboratory equipment to ensure the traceability of the experiments, for instance, an industrial thermal-vacuum chamber, more robust than used in Figure 10. It is also necessary that the regulations of small CubeSat satellites be used as a reference, sufficiently documented and, in turn, applied to functional prototypes, given that in relation to CanSat developments, the available documentation is mostly of an educational and exploratory nature, and there is no standardized testing methodology yet available

(2) Thanks to implementing the modular design methodology, which is reflected in how the different subsystems were conceived (see Figures 3–5), it was possible to guarantee data communication, energy transfer, and structure of the module. Having a standardized bus in the interconnection architecture between the different subsystems allows the module to support a wide variety of experiments or payloads (sensors)

(3) In this particular case, the testing of the Simple-2 module enabled the verification of the TRL (technology readiness level) of the design and technology implemented, since, in this prototype, level 4 (component and/or breadboard laboratory validated), level 5 (component and/or breadboard validated in simulated or real-space environment), and level 6 (system adequacy validated in simulated environment) were satisfied. In light of these levels, the Simple-2 module is postulated as a platform subject to a redesigning and debugging process for future developments. By conducting the test in a real operating environment using high-altitude balloons, also, it was possible to corroborate the correct operation of acquisition, power consumption, and telemetry of the unit in extreme environments, given the results in Figures 16 and 17. Furthermore, the obtained variables showed amplitudes and result consistent with the tests previously conducted in controlled experimental environments

(4) The increase in some variables' uncertainty is due to not adopting all the recommendations found in the references. In the CanSat Simple-2, these recommendations were ignored due to conditions in the installed capability available both in the academy and in the local industry for aerospace projects. However, through the development of vibration and shock tests, frequency ranges were observed for which devices with masses ≤ 1 kg such as CanSats did not reveal resonances (see Figure 15), corroborating that these CanSats have a dynamic response in the operating ranges that commonly are found in space launchers

In conclusion, having metrological processes and qualification testing environments improves these devices' reliability

and enhances their use, not only in traditional academic and educational contexts but also in the commercial sector. Using these aerospace design criteria guarantees both the diversification and the use of applications in ground-air scenarios for remote sensing activities, thereby promoting technological development that will enable the emerging economies of Latin America to access to space.

Data Availability

The data used to support the findings of this study are included within the supplementary materials file.

Conflicts of Interest

The authors declare no conflict of interest.

Acknowledgments

The authors would like to acknowledge the support of the Oficina de Asuntos Espaciales of the FAC (Fuerza Aerea Colombiana) gratefully. Their guidance for developing flight tests and adequate airspace use according to regulations and their logistical support with the sonde's launch until its recovery were extremely helpful. The authors also want to extend their acknowledgments to the Metrology and Microengineering laboratories at Universidad EAFIT for providing the necessary equipment to carry out this research. The authors also would like to extend special thanks to the Colombian companies A-MAQ S.A.S for allowing the use of their facilities and equipment and their technical advice to develop the sinusoidal vibration and Cryogas-Air Products Colombia company for providing the ascent gas for the flight test. Finally, the authors would like to express thanks to the future generation of young researchers who participated in this mission and contributed to various activities in the Rocketry and Propulsion Study Research Group. This project was funded by the Vicerrectoría de Descubrimiento y Creación, through the Dirección de Planeación y Descubrimiento Formativo at Universidad EAFIT as well as with resources of researchers and groups involved.

Supplementary Materials

Supplementary description. Readme.rtf: file related to the dataset of the tests presented in this work. *(Supplementary Materials)*

References

[1] R. J. Twiggs, *Introducing New Challenges for Future Space Missions*, International CanSatWorkshop, 2007.

[2] Á. Colín, B. Bermúdez Reyes, G. E. Morrobel et al., "Construcción de un picosatélite cansat," *Ciencia UANL*, vol. 19, no. 81, pp. 34–38, 2016.

[3] R. Walker, P. Galeone, H. Page et al., "ESA hands-on space education project activities for university students: attracting and training the next generation of space engineers," in *IEEE EDUCON 2010 Conference*, pp. 1699–1708, Madrid, Spain, 2010.

[4] M. Sweeting, "Modern small satellites-changing the economics of space," *Proceedings of the IEEE*, vol. 106, no. 3, pp. 343–361, 2018.

[5] H. J. Kramer and A. P. Cracknell, "An overview of small satellites in remote sensing," *International Journal of Remote Sensing*, vol. 29, no. 15, pp. 4285–4337, 2008.

[6] J. S. Triana, S. Bautista, and F. A. Díaz González, "Identification of design considerations for small satellite remote sensing systems in low earth orbit," *Journal of Aerospace Technology and Management*, vol. 7, no. 1, pp. 121–134, 2015.

[7] LibreCube, "LibreCube, a open source space and earth exploration," 2020, April 2020, https://librecube.org/.

[8] A. Scholz and J. N. Juang, "Toward open source CubeSat design," *Acta Astronautica*, vol. 115, pp. 384–392, 2015.

[9] D. Tarasick, T. Carey-Smith, W. Hocking et al., "Quantifying stratosphere-troposphere transport of ozone using balloon-borne ozonesondes, radar windprofilers and trajectory models," *Atmospheric Environment*, vol. 198, pp. 496–509, 2019.

[10] A. Y. Botero, J. S. Rodríguez, J. G. Serna, A. Gómez, and M. J. García, "Design construction and testing of a data transmission system for a mid-power rocket model," in *2017 IEEE Aerospace Conference*, pp. 1–14, Big Sky, MT, 2017.

[11] A. Yarce, J. S. Rodríguez, J. Galvez, A. Gómez, and M. J. García, "Simple-1: development stage of the data transmission system for a solid propellant mid-power rocket model," *Journal of Physics: Conference Series*, vol. 850, article 012019, 2017.

[12] L. M. Reyneri, C. Sansoè, C. Passerone et al., "Design solutions for modular satellite architectures," in *Aerospace Technologies Advancements*, InTech Editor, 2010.

[13] B. M. O. Nunes, *The design and testing of a picosatellite, the TubeSatellite CTSAT-1 [Ph.D. thesis]*, Universidade Nova de Lisboa, 2019.

[14] J. Dennison, G. Wilson, A. Souvall, B. Russon, and K. Gamaunt, *CubeSat Space Environments Effects Studied in the Space Survivability Test Chamber*, Poster in Materials Physics at DigitalCommons, Utah State University, 2016.

[15] G. Obiols-Rabasa, S. Corpino, R. Mozzillo, and F. Stesina, "Lessons learned of a systematic approach for the e-st@ r-II CubeSat environmental test campaign," in *Proceedings of the 66th International Astronautical Congress*, Jerusalem, Israel, October 2015.

[16] H. Masui, T. Hatamura, and M. Cho, "Testing of Micro/Nano Satellites and Their On-Orbit Performance," in *27th Annual AIAA/USU Conference on Small Satellites*, Logan, Utah, 2013.

[17] N. Bean, "A Modular Small Satellite Bus for Low Earth Orbit Missions," in *2nd Annual AIAA/USU Conference on Small Satellites*, Logan, Utah, 1988.

[18] S. Wei-Xu, Z. Ke-ke, L. Chun-Peng, and S. Rui-Feng, "Research on the design method of modular structure for satellites," in *Proceedings of the 1st International Conference on Mechanical Engineering and Material Science*, Atlantis Press, 2012.

[19] M. Oredsson, *Electrical power system for the CubeSTAR nanosatellite, [M.S. thesis]*, University of Oslo, 2010.

[20] J. R. Berrendero, "TEMA 1,Diseño de experimentos: modelo unifactorial. Análisis de Datos - Grado en Biología Universidad Autónoma de Madrid," 2017, http://verso.mat.uam.es/~joser.berrendero/cursos/adatos/ad2-tema1-12.pdf.

[21] W. W. Burchett, A. R. Ellis, S. W. Harrar, and A. C. Bathke, "Nonparametric inference for multivariate data: the R package

npmv," *Journal of Statistical Software*, vol. 76, no. 4, pp. 1–18, 2017.

[22] U. de Cordoba, "Universidad de Cordoba," 2017, http://www.uco.es/zootecniaygestion/img/pictorex/16_11_29_8_multivariante.pdf.

[23] F. Muñoz, *Curso de Estadística no-paramétrica Sesión 3: Regresión no paramétrica y Contrastes de Aleatoriedad y bondad de ajuste*, Departamento de Estadística, Universitat de Valéncia, 2013.

[24] J. Readman, S. Pollard, C. N. Hewitt et al., "An introduction to pollution science," in *The Royal Society of Chemistry*, pp. i–332, RSC Publishing, 2006.

[25] A. W. Bowman and A. Azzalini, *Applied smoothing techniques for data analysis: the kernel approach with S-Plus illustrations*, vol. 18, OUP Oxford, 1997.

[26] (IDEAM)Instituto de Hidrología, *M.y.E.A. Glosario*, 2017, http://www.ideam.gov.co/web/atencion-yparticipacion-ciudadana/glosario.

[27] I. Yunis, "The standard deviation of launch vehicle environments," in *46th AIAA/ASME/ASCE/AHS/ASC Structures, Structural Dynamics and Materials Conference Structural*, Austin, Texas, 2005.

[28] A. Mehrparvar, D. Pignatelli, J. Carnahan et al., *CubeSat Design Specification Rev 13*, The CubeSat Program, Cal Poly San Luis Obispo, US, 2014.

[29] G. Fernandes, M. Santos, V. Silva, J. Almeida, and P. Nogueira, "Thermal tests for CubeSat in Brazil: lessons learned and the challenges for the future," in *Proceedings of the 67th International Astronautical Congress*, vol. 27, Guadalajara, Mexico, 2016.

[30] R. S. S. Chisabas, D. F. Cantor, G. Loureiro, and C. D. O. Lino, "Method for CubeSat thermal-vacuum cycling test specification," in *47th International Conference on Environmental Systems*, Charleston, South Carolina, 2017.

[31] M. M. Finckenor and K. Groh, "A researcher's guide to: space environmental effects," *National Aeronautics and Space Administration International Space Station Researcher's Guide Series, Houston, Texas*, p. 15, 2015, NP-2015-03-015-JSC.

[32] D. Wernham and A. Piegari, "Optical coatings in the space environment," in *Optical Thin Films and Coatings*, pp. 789–811, Elsevier, 2018.

[33] Standard G. E. V., *NASA Publication GSFC-STD-7000, General Environmental Verification Standard, NASA, Goddard Space Flight Center, Maryland*, 2005.

[34] D. Handbook, *304A (USAF):"Test Requirements for Launch, Upper-Stage, and Space Vehicles, Volume II: Application Guidelines"*, US Air Force (AF), Air Force Space Command, El Segundo, California, 1999.

[35] E. Secretariat, *ESA-ESTEC, Requirements & Standards Division. Space Engineering Testing*, p. 29, 2013, https://ecss.nl/standard/ecss-e-st-10-03c-testing/.

[36] E. Perl, "Test requirements for launch, upper-stage, and space vehicles," Aerospace Report No. Technical report, The Aerospace Corporation TR-2004 (8583)-1-REV-A, El Segundo, CA, 2006.

[37] NASA, *Launch Services Program Level Dispenser and CubeSat Requirements Document*, National Aeronautics and Space Administration, 2014.

[38] T. Sarafin, P. Doukas, L. Demchak, and M. Browning, *Vibration Testing of Small Satellites: Part 1: Introduction to Vibration Testing*, Instar Engineering and Consulting, Inc, 2017.

[39] S. S. Rao, *Mechanical Vibrations Fifth Edition*, Pearson Education, Miami, 2011.

[40] T. Irvine, *An Introduction to the Shock Response Spectrum*, Rev P, Vibrationdata, 2002.

[41] J. Amat, *Prueba de los rangos con signo de Wilcoxon*, 2016, https://rpubs.com/Joaquin_AR/218464.

[42] M. Brummitt, *Development of CubeSat Vibration Testing Capabilities for the Naval Postgraduate School and Cal Poly, [M.S. thesis]*, California Polytechnic State University, San Luis Obispo, California, 2010.

[43] S. Hanly, *Shock Vibration Testing Overview eBook*, Mide Technology, 2016.

[44] T. Sarafin, L. Demchak, P. Doukas, and M. Browning, *Vibration Testing of Small Satellites Part 5: Random Vibration Testing*, Instar Engineering and Consulting, Inc, 1967.

[45] D. Davis, N. Awwad, and T. Fitzgerald, "Test requirements for launch, upper-stager and space vehicles," Technical Report, SMC-S-016, 2014.

[46] J. Amat, *Correlación lineal y Regresión lineal simple*, 2016, https://rpubs.com/Joaquin_AR/223351.

[47] E. G. Portugués, *A Short Course on Nonparametric Curve Estimation*, 2018, https://bookdown.org/egarpor/NP-EAFIT/.

[48] J. H. McDonald, *Handbook of biological statistics; Vol. 2*, Sparky House Publishing Baltimore, MD, 2009.

[49] J. A. Rodrigo, *Validación de modelos de regresión: Cross-validation, OneLeaveOut, Bootstrap*, 2016, https://rpubs.com/Joaquin_AR/238251. 17-08-2018.

[50] E. G. Portugués, *MSc in Big Data Analytics at Carlos III University of Madrid*, 2019, https://bookdown.org/egarpor/PM-UC3M/, 23-01-2019.

[51] G. James, D. Witten, T. Hastie, and R. Tibshirani, *An Introduction to Statistical Learning; Vol. 112*, Springer, 2013.

[52] C. G. Martínez, *Métodos De Regresión No Lineal*, 2018, https://rpubs.com/Cristina_Gil/Regr_no_lineal, 12-12-2018.

[53] P. Delicado, *Curso demodelos no paramétricos*, Departament d'Estadística i Investigació Operativa, Universitat Politécnica de Catalunya, 2008.

[54] N. B. Abdelkade, *Regresión no paramétrica en R [M.S. thesis]*, Estadística Aplicada, Universidad de Granada, Spain, 2009.

[55] C. G. Martínez, *Técnicas de regulariación y selección del mejor modelo*, 2018, https://rpubs.com/Cristina_Gil/Regularizacion_Seleccion, 09-09-2018.

[56] J. Olaya, J. Reina, L. L. Torres, M. C. Paz, and L. A. Pereira, "Nonparametric modeling of the eight-hour average air pollution due to carbon monoxide and tropospheric ozone," *Ingeniería y Competitividad*, vol. 16, pp. 147–157, 2014.

[57] A. J. Flórez, "CO atmospheric concentration modeling using nonparametric regression with non-homogeneous variability bands," *Ingeniería y Competitividad*, vol. 16, pp. 273–281, 2014.